NADC-77250-30

LEVEL II

12

EVALUATION OF EQUIVALENT INITIAL FLAWS FOR DAMAGE TOLERANCE ANALYSIS

R. C. Rice
D. Broek
BATTELLE
Columbus Laboratories
505 King Avenue
Columbus, Ohio 43201

30 September 1978

Final Report for Period 30 September 1977 — 30 September 1978

Approved for public release; distribution unlimited.

Prepared for

NAVAL AIR DEVELOPMENT CENTER
Warminster, Pennsylvania 18974

NOTICES

REPORT NUMBERING SYSTEM - The numbering of technical project reports issued by the Naval Air Development Center is arranged for specific identification purposes. Each number consists of the Center acronym, the calendar year in which the number was assigned, the sequence number of the report within the specific calendar year, and the official 2-digit correspondence code of the Command Office or the Functional Directorate responsible for the report. For example: Report No. NADC-78015-20 indicates the fifteenth Center report for the year 1978, and prepared by the Systems Directorate. The numerical codes are as follows:

CODE	OFFICE OR DIRECTORATE
00	Commander, Naval Air Development Center
01	Technical Director, Naval Air Development Center
02	Comptroller
10	Directorate Command Projects
20	Systems Directorate
30	Sensors & Avionics Technology Directorate
40	Communication & Navigation Technology Directorate
50	Software Computer Directorate
60	Aircraft & Crew Systems Technology Directorate
70	Planning Assessment Resources
80	Engineering Support Group

PRODUCT ENDORSEMENT - The discussion or instructions concerning commercial products herein do not constitute an endorsement by the Government nor do they convey or imply the license or right to use such products.

APPROVED BY: Edward J. Sturm DATE: 30 Nov 1978

EDWARD J. STURM
CDR USN

NADC-77250-30

EVALUATION OF EQUIVALENT INITIAL FLAWS FOR DAMAGE TOLERANCE ANALYSIS

R. C. Rice
D. Broek
BATTELLE
Columbus Laboratories
505 King Avenue
Columbus, Ohio 43201

30 September 1978

Final Report for Period 30 September 1977 – 30 September 1978

Approved for public release; distribution unlimited.

Prepared for

Naval Air Development Center
Warminster, Pennsylvania 18974

Unclassified

SECURITY CLASSIFICATION OF THIS PAGE (When Data Entered)

REPORT DOCUMENTATION PAGE

READ INSTRUCTIONS BEFORE COMPLETING FORM

1. REPORT NUMBER (18) NADC-77250-30 (19) | 2. GOVT ACCESSION NO. | 3. RECIPIENT'S CATALOG NUMBER

(9) Final rept. 30 Sep 77 – 30 Sep 78

4. TITLE (and Subtitle) (6) (14)

EVALUATION OF EQUIVALENT INITIAL FLAWS FOR DAMAGE TOLERANCE ANALYSIS

5. TYPE OF REPORT & PERIOD COVERED
Final Report 9/30/77 – 9/30/78

6. PERFORMING ORG. REPORT NUMBER
BATT-G-6496

7. AUTHOR(s) (10)

R. C. Rice and D. Broek

8. CONTRACT OR GRANT NUMBER(s) (15)
N62269-77-C-0543 new

9. PERFORMING ORGANIZATION NAME AND ADDRESS
Batelle Columbus Laboratories
505 King Avenue
Columbus, Ohio 43201

10. PROGRAM ELEMENT, PROJECT, TASK AREA & WORK UNIT NUMBERS

11. CONTROLLING OFFICE NAME AND ADDRESS (11) 30
Naval Air Development Center
Warminster, Pennsylvania 18974

12. REPORT DATE
September 30, 1978

13. NUMBER OF PAGES
68

14. MONITORING AGENCY NAME & ADDRESS (if different from Controlling Office) (12) 76p.
DCASMA
Defense Electronics Supply Center
Building 5, 1502 Wilmington Pike
Dayton, Ohio 45444

15. SECURITY CLASS. (of this report)
Unclassified

15a. DECLASSIFICATION/DOWNGRADING SCHEDULE

16. DISTRIBUTION STATEMENT (of this Report)

Approved for public release; distribution unlimited

17. DISTRIBUTION STATEMENT (of the abstract entered in Block 20, if different from Report)

Approved for public release; distribution unlimited

18. SUPPLEMENTARY NOTES

19. KEY WORDS (Continue on reverse side if necessary and identify by block number)

initial crack, fatigue crack initiation, fatigue crack propagation
equivalent initial flaw, intermetallic particles

20. ABSTRACT (Continue on reverse side if necessary and identify by block number)

An experimental investigation was conducted to establish whether the size of the so-called equivalent initial flaw can be rationalized on the basis of the size of intermetallic particles (or clusters of such) in the material. Fatigue experiments were conducted on flat specimens with a central hole cut from 7075-T73 Al alloy plate. The size and number of intermetallic particles were measured in the regions where crack initiation was anticipated. Assuming the existence of an "equivalent initial flaw" the fatigue life of the

(over)

DD FORM 1 JAN 73 1473 EDITION OF 1 NOV 65 IS OBSOLETE
S/N 0102-014-6601

Unclassified 404020

SECURITY CLASSIFICATION OF THIS PAGE (When Data Entered)

20.

specimens was calculated by means of crack growth analysis. In this manner the size of the equivalent initial flaw was determined as the flaw that needs to be assumed present from the beginning to give a crack propagation life equal to the observed life of the specimen. The sizes of equivalent initial flaws so calculated did not show a correlation with number or size of intermetallic particles.

SUMMARY

The importance of equivalent initial flaws (EIF) in damage tolerance analysis is discussed and the rationale behind an evaluation of their physical reality is presented. Details of an experimental program and metallographic analysis are included along with a statistical analysis of generated data.

Program results on a 7075-T73 plate material do not indicate a meaningful correlation between the distribution of EIF values and the distribution of intermetallic particles. Test results do supply additional data on small cracks in holes, however, which are useful for statistically defining empirical EIF values. The empirically established EIF values ranged from 0.0005 to 0.0036 inch (13 to 90 μm) for 19 experimental results. When ranked, the computed values of EIF followed a logarithmically linear cumulative frequency pattern which allowed projection of an EIF of 0.0045 inch (115 μm) for a failure rate of 1 in 100.

PREFACE

This research program was conducted in the Structures and Mechanics Research Department, Battelle's Columbus Laboratories, Columbus, Ohio, under Contract No. N62269-77-C-0543. The program was administered by the Aircraft and Crew Systems Technology Directorate, Naval Air Development Center, Warminster, Pennsylvania, with Mr. Paul Kozel providing technical liaison. This report summarizes work performed during the period September 30, 1977, through September 30, 1978.

The experimental portions of this research program were accomplished by Messrs. James E. Wood and Norman D. Frey of the Fatigue and Fracture Technology Laboratories. The optical metallography performed in this program was done by Mr. Lee Dillinger, while assistance in using the scanning electron microscope was given by Mr. Andrew Skidmore. Precision machining required in specimen preparation was done by Mr. Robert F. Fletcher. The use of the image analyzer of the National Aerospace Institute, Holland, is gratefully acknowledged.

CONTENTS

LIST OF ILLUSTRATIONS

LIST OF ILLUSTRATIONS

LIST OF ILLUSTRATIONS

LIST OF TABLES

1. INTRODUCTION

The United States Air Force's new damage tolerance requirements per MIL-A-83444 stipulate that initial damage shall be assumed present in an aircraft structure. More specifically, an 0.005-inch (.125 mm) initial flaw is assumed at every structural hole, whereas at critical locations, the initial damage at a hole is assumed to be an 0.02-inch (0.5 mm) or an 0.05-inch (1.25 mm) crack depending upon the type of structure.

The assumption of initial damage is made to insure the safety of the structure. This does not necessarily imply that the fatigue life to crack initiation is completely ignored, since this would mean sacrificing a substantial part of the useful fatigue life. It is possible to select ths size of the initial flaw in such a manner that if a flaw of that size were present its propagation to failure would result in the same fatigue life as is observed for a virtually crack-free specimen. Thus, the assumed initial flaw is not a real crack, but an equivalent crack which gives fatigue life equivalent to that of an uncracked part. As such, the equivalent initial flaw (EIF) when used in this manner is no more than a mathematical convenience which permits fatigue life prediction by means of crack-growth analysis only. It eliminates the need for a combined fatigue-life analysis and crack-growth analysis.

If the above approach is to be considered in design, the equivalent initial flaw size has to be known. The damage tolerance requirements of MIL-A-83444 assume a very large EIF, which is based on a conservative analysis of fatigue data. However, if the EIF is a viable concept, it would be worthwhile if it could be given a physical basis, so that the size of the EIF could be obtained from a measurable physical quantity instead of from an empirical study.

Since the fatigue life of a part or coupon with a hole is affected by burrs and scratches, it seems feasible that the EIF can be correlated with the quality of the hole. This is the approach presently pursued by the USAF.

Many experimentalists [e.g., 1-3]* have observed that fatigue cracks are often initiated at inclusions or second phase particles in the material. The inclusion or particle may break [4] or lose coherence [2] and thus introduce an (initial) crack or flaw. Therefore, it was worthwhile to investigate whether the size of particles determines the size of the EIF. The statistical nature of the distribution of particles and their variable size would determine the probability of a (large) particle being intercepted by the edge of the hole at the point of highest stress. Thus, it seemed likely also that the scatter in fatigue life (i.e., the statistical population of EIF) might be related to the particle statistics.

The objective of the work reported here was to investigate whether particles can indeed be correlated with the EIF. To this effect fatigue tests were run on coupons with a central hole. The particle content of the material, 7075-T73 plate, was first characterized. Also, the particle distribution at the edge of the holes was carefully recorded. Finally, it was checked whether the size of the EIF was in accordance with particle size. The results were negative, in the sense that it was established that particles appear to play no dominant role in the initiation of a fatigue crack at a hole (although they may in smooth specimens).

This report is organized to first give a detailed description of the research program, then follows the statistical characterization of the particle content of the material used for the experiments. Subsequently, the distribution of particles at the edges of the holes in the test specimens are discussed. Thereafter, follow the experimental results and a review of the fractographic observations at the crack initiation sites. Finally, the concept of the EIF and its relation to particle size and distribution are discussed in detail.

---

* References are listed on page 67.

2. RESEARCH PROGRAM

This research program was initiated to determine whether a correlation exists between the size of intermetallic particles in a structural aluminum alloy and the size of an equivalent initial flaw that could be used in a crack-growth analysis to predict fatigue failure. The basic premise behind this idea was that intermetallic particles (or clusters of smaller particles) actually could be viewed as inherent flaws or microcracks in the material. Considering a random distribution of particle sizes and locations, it was presumed that a component with a large intermetallic particle (i.e., flaw) in a highly stressed region of that component would fail before a similar component without metallurgical discontinuities in critical areas. If true, this concept would help explain the scatter typically seen in fatigue data and allow more realistic fatigue-life estimates.

The experimental program described in the following sections was devised to evaluate the relationship between intermetallic particles and equivalent initial flaws. The initial task was to characterize the intermetallic particle distributions in the 7075-T73, 0.250-inch-thick plate chosen for this study. Once the particle distributions were quantified for the overall plate, center-hole specimens were manufactured. The specimens were designed in such a way as to promote crack initiation at the hole/plate surface interface where the intermetallic particle distributions could be documented. These specimens were then fatigue cycled under constant amplitude load conditions until cracks initiated at the front corner of the hole, at which time, the crack initiation site was photographed through an optical microscope. Subsequently, the specimens were reloaded into the fatigue system and cycled to failure while monitoring crack extension. After all fatigue testing was completed, each of the fracture surfaces were examined with a scanning electron microscope. Finally, the crack initiation and propagation data were reviewed in the context of an equivalent initial flaw. Each of these phases are elaborated upon in the following sections.

Statistical Definition of Intermetallic Particles

The distribution of intermetallic particles in the 7075-T73 plate material were determined in the Battelle metallography laboratory and the National Aerospace Laboratory (NLR) in the Netherlands. The NLR equipment was used in addition to the Battelle facilities because it has a computerized image analyzer which permitted examination of a large number of image fields. The data from these two investigations and an interpretation of the results follow in the next few paragraphs.

NLR Image Analyzer Results

The NLR in the Netherlands provided, on a gratis basis, access to their automated image analyzer which scanned 2000 image fields on each sample using seven intermetallic particle size classes. In addition to particle size, the analyzer also computed mean free distance between particles and the total area of particles. Each field was 2.65 by 3.54 mils* (67 x 90 μm) and the total area scanned on each sample was 50 fields wide or 0.132 inch, by 40 fields long or 0.142 inch (3.60 mm), for a total viewing area of 0.0187 inch^2 (12.06 mm^2). Two different samples were examined, both in the X-Y plane (or rolled surface) of the plate. The data obtained were transferred to punched cards for computer analysis.

The data were analyzed in several ways. First, computer generated maps were drawn that reflected the size distribution of particles and the density of particle clusters. For example, Figures 2.1 through 2.4 demonstrate the distribution of particles greater than .095, .235, and .380 mils (2.4, 4.8, 6.0, and 9.6 μm) in length, respectively, for Sample A2. Similarly, Figure 2.5 shows the density of particles (by percent projected area) for the 0.0187 inch^2 (12.06 mm^2) area scanned on Sample A2. These figures illustrate a more or less random distribution of intermetallic particles, most of which are less than 0.1 mil (2.4 μm) in length, and which represent less than 5 percent of the area of 99 percent of the scanned image fields. A similar trend was observed on Sample B2. These results indicated that the intermetallic particles being examined were quite small (at least relative to currently used EIF sizes) and that they were quite diverse.

* 1 mil = 0.001 inch.

Each unit value represents 2 particles

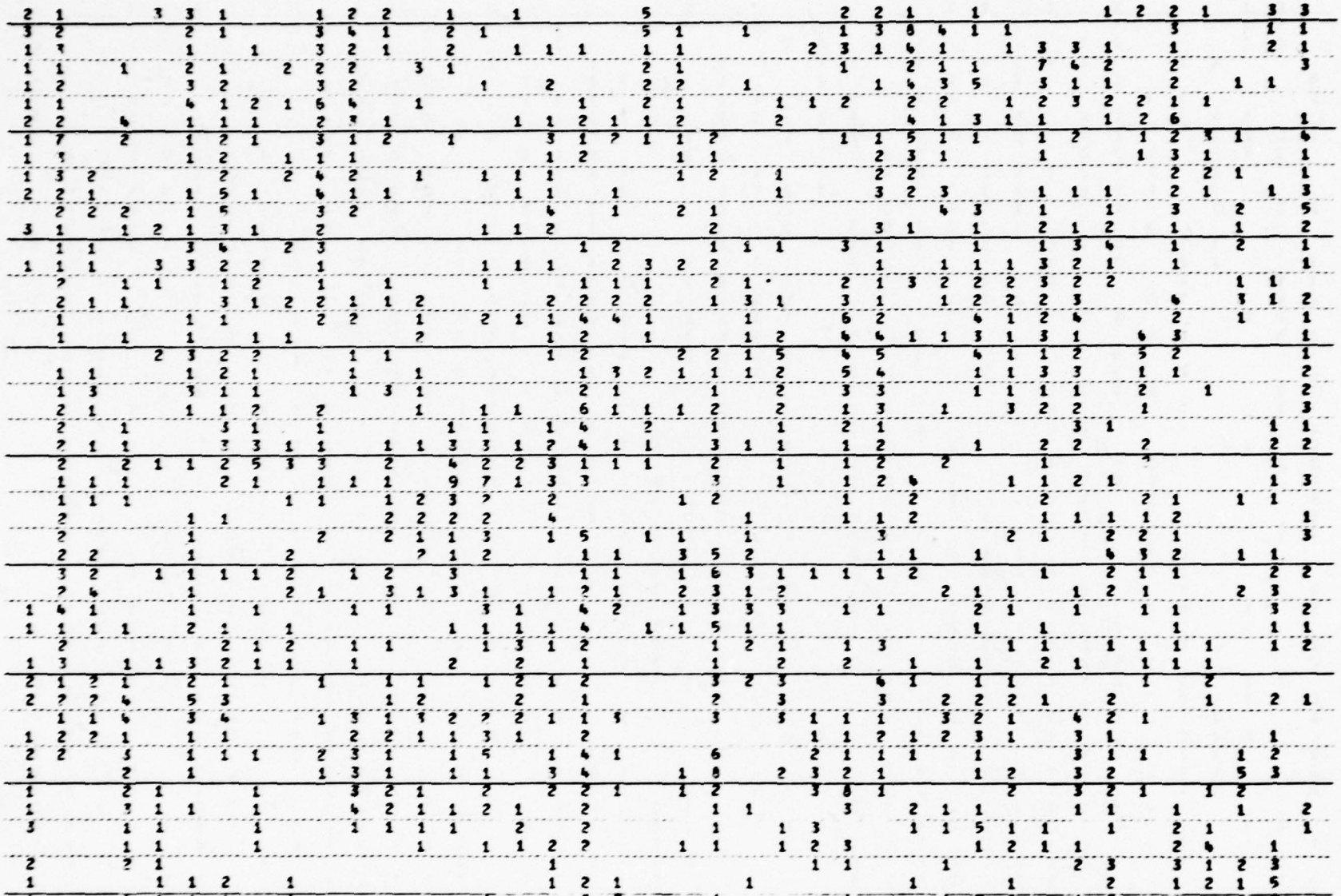

FIGURE 2.1. MATRIX OF TOTAL NUMBER OF PARTICLES PER FIELD GREATER THAN 2.4 MICRONS IN SIZE

Each unit value represents 1 particle

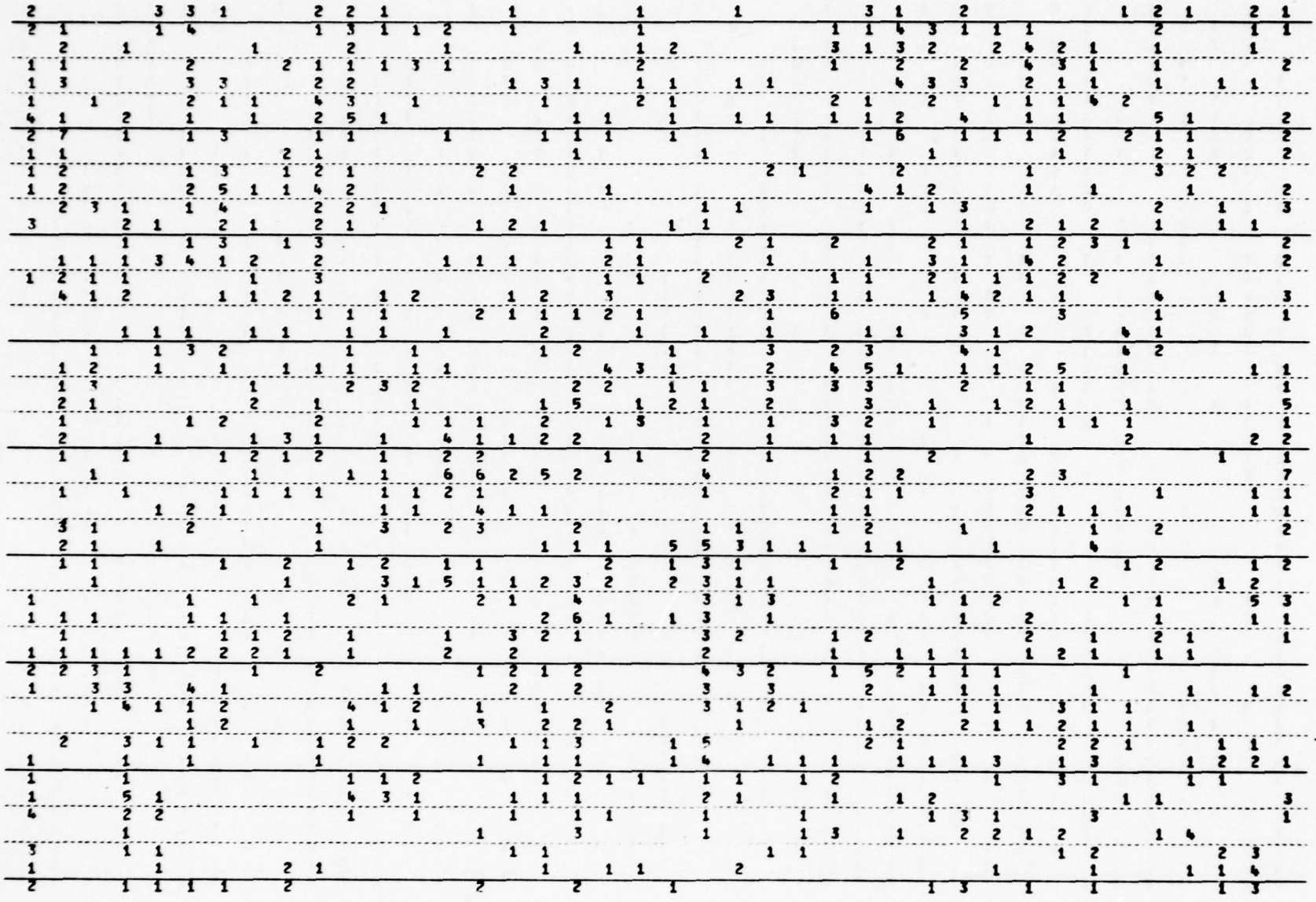

FIGURE 2.2. MATRIX OF TOTAL NUMBER OF PARTICLES PER FIELD GREATER THAN 4.8 MICRONS IN SIZE

Each unit value represents 1 particle

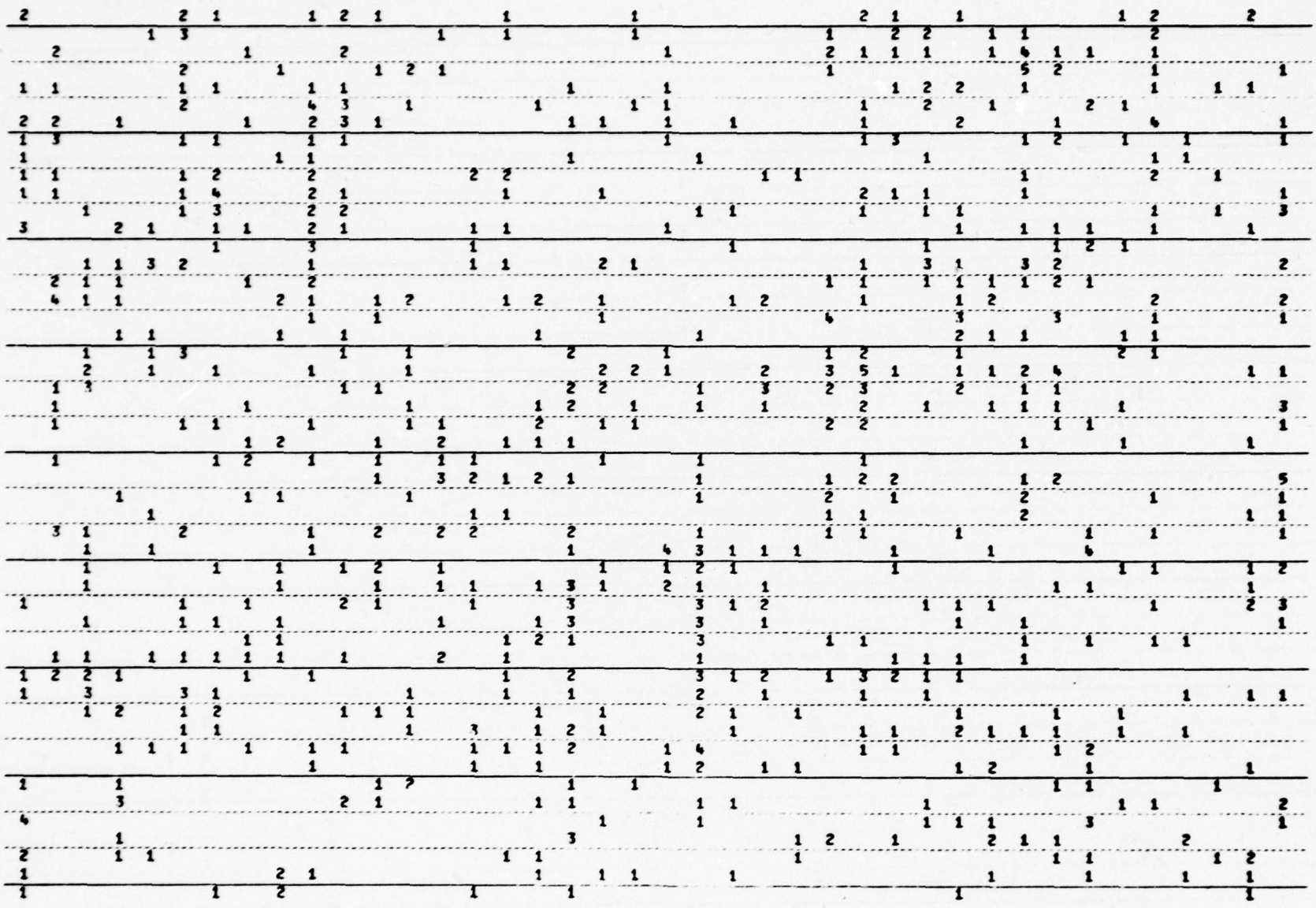

FIGURE 2.3. MATRIX OF TOTAL NUMBER OF PARTICLES PER FIELD GREATER THAN 6.0 MICRONS IN SIZE

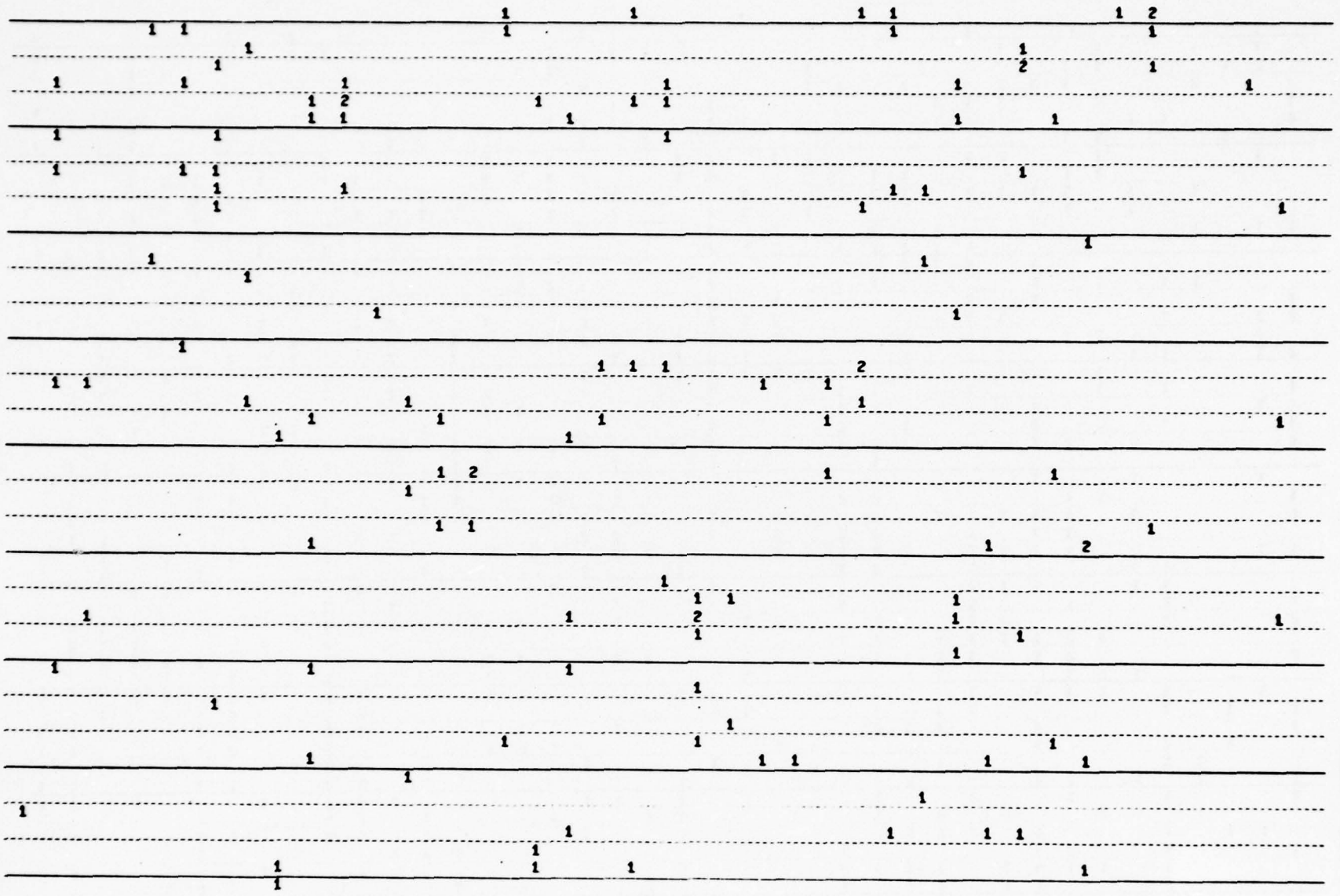

FIGURE 2.4. MATRIX OF TOTAL NUMBER OF PARTICLES PER FIELD GREATER THAN 9.6 MICRONS IN SIZE

NADC-77250-30

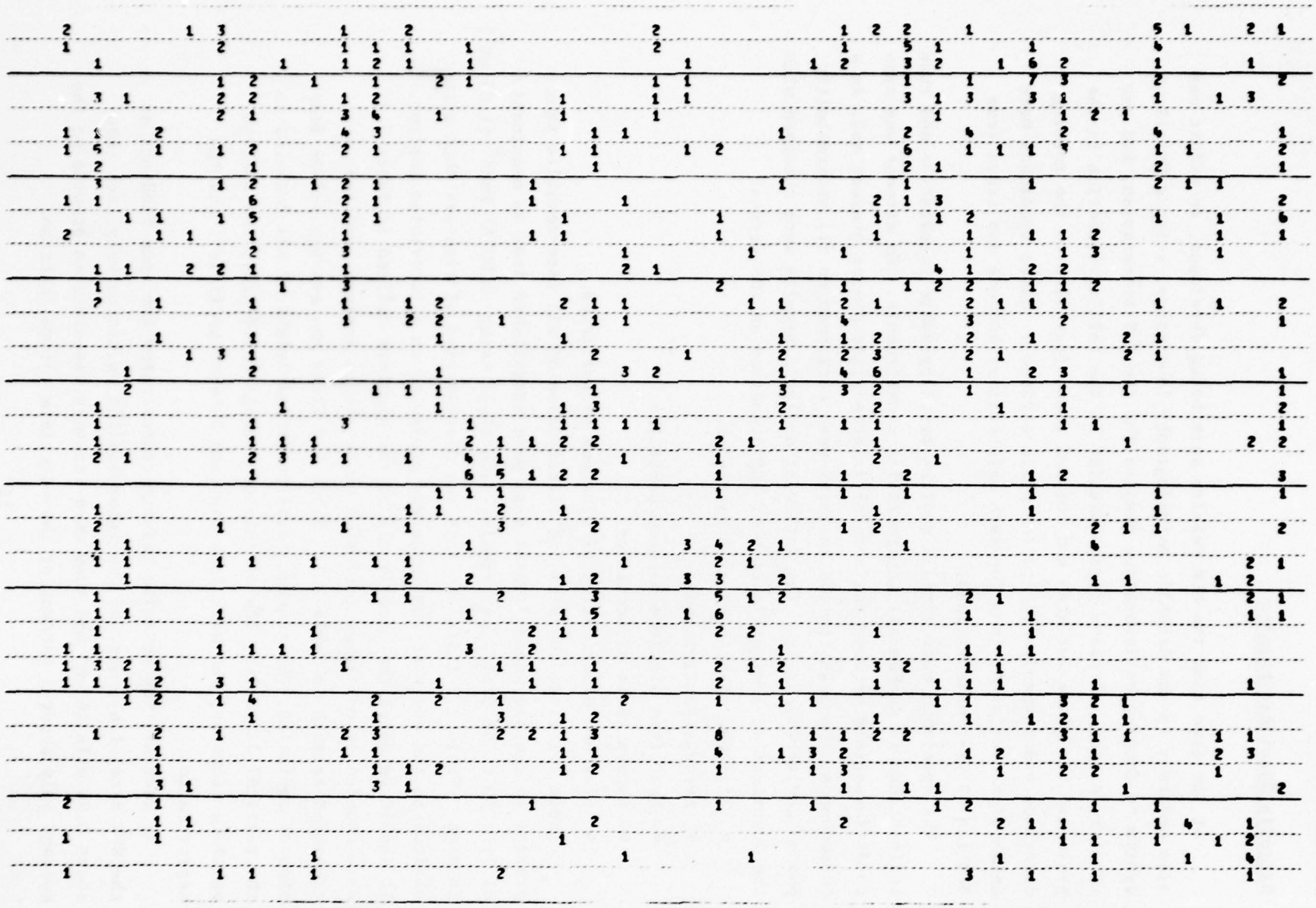

FIGURE 2.5. PERCENTAGE AREA OF PARTICLES PER FIELD – ROUNDED TO THE NEAREST PERCENT

Battelle Quantimet Results

At the same time the NLR results were being developed, an effort was also underway in the Battelle metallography laboratory, using a Quantimet system to develop collaborative results for the X-Y orientation, and new results for the Y-Z plane (perpendicular to the rolling direction in the plate and the plate surface) and the X-Z plane (parallel to the rolling direction and perpendicular to the plate surface). Three specimens were taken from Section A2 (one for each orientation) and one was taken from Section B2 (X-Y orientation).

The specimens were given a routine metallographic preparation and then stain-etched to darken all intermetallic constituents. No attempt was made to differentiate between the several intermetallic phases present and, as a consequence, the quantitative analyses were performed on all intermetallic phases indiscriminately. The following analysis results were obtained with the Quantimet at a magnification of 180 diameters on the screen:

- Size and distribution of particles
- Average particle size
- Mean free distance between particles
- Aspect ratio of particles
- Size and distribution of clusters of particles.

Table 2.1 lists the size and distribution of all intermetallic phases present in the specimens. These data were established from an examination of from 30 to 48 fields per sample, each field being 0.00287 inch^2 (1.85 mm^2) in area. Table 2.2 lists the size and distribution of clusters that were obvious to the eye when the image was projected on a television monitor. It should be noted that nearly all of the clusters defined in Table 2.2 were counted as one large inclusion by the image analyzer and they are tabulated as such in Table 2.1. Table 2.3 lists the average volume fraction of particles, the average total projected height of all features in the vertical direction, the calculated average chord size, the average particle diameter, the mean free distance between particles, and the aspect ratio.

In general, the Battelle results demonstrated the same findings as the NLR data, i.e., most of the intermetallic particles were less than about 0.24 mils (6 μm) and they were randomly dispersed to provide on the average only about 2 percent of the materials volume fraction.

TABLE 2.1. SIZE AND DISTRIBUTION OF INTERMETALLIC PHASES IN 7075 ALUMINUM PLATE

Number of particles in each class range

Mils	Range (microns)	Preparation A 2			Preparation B 2
		x-y	x-z	y-z	X-Y
<0.12	(< 3)	11489	8911	10989	12933
0.12 - 0.24	(3-6)	5035	6114	6826	4784
0.24 - 0.35	(6-9)	1935	2970	3058	1472
0.35 - 0.47	(9-12)	824	1119	1103	510
0.47 - 0.59	(12-15)	345	594	491	181
0.59 - 0.71	(15-18)	206	326	225	90
0.71 - 0.83	(18-21)	73	142	95	36
0.83 - 0.94	(21-24)	57	66	38	19
0.94 - 1.06	(24-27)	26	34	22	5
1.06 - 1.18	(27-30)	31	18	5	6
1.18 - 1.30	(30-33)	11	16	9	1
1.30 - 1.42	(33-36)	8	6	1	1
1.42 - 1.54	(36-39)	1	8	4	2
1.54 - 1.65	(39-42)	10	5	0	-
1.65 - 1.77	(42-45)	1	1	1	
1.77 - 1.89	(45-48)	5	0	1	
1.89 - 2.01	(48-51)	4	1	-	
2.01 - 2.13	(51-54)	1	1		
2.13 - 2.24	(54-57)	-	-		
	Total	20062	20332	22868	20040

TABLE 2.2. SIZE AND DISTRIBUTION OF CLUSTERS

Mils	Range (microns)	Preparation A 2			Preparation B 2
		x-y	x-z	y-z	X-Y
1.71 - 0.83	(18-21)	6			
0.83 - 0.94	(21-24)	12	1		
0.94 - 1.06	(24-27)	12	9		3
1.06 - 1.18	(27-30)	21	4	1	4
1.18 - 1.30	(30-33)	10	4	3	1
1.30 - 1.42	(33-36)	8	4	1	0
1.42 - 1.54	(36-39)	1	7	3	2
1.54 - 1.65	(39-42)	10	3	0	-
1.65 - 1.77	(42-45)	1	1	1	
1.77 - 1.89	(45-48)	5	0	1	
1.89 - 2.01	(48-51)	4	1	-	
2.01 - 2.13	(51-54)	1	1		
		-	-		
	Total	92	35	10	10

TABLE 2.3. AVERAVE V/O OF PARTICLES, AVERAGE TOTAL PROJECTED HEIGHT OF FEATURES, AVERAGE CALCULATED CHORD SIZE, AVERAGE CALCULATED DIAMETER OF FEATURES, MEAN FREE DISTANCE BETWEEN PARTICLES AND ASPECT RATIO

Preparation Identification	Orientation	Volume Fraction v/o, percent	Projected Height, P_y	Chord Size $\bar{c}$(a)		Average Particle Diameter d(b)		Mean Free Distance MFD(c)		Particle Aspect Ratio
				mil	(μ)	mil	(μ)	mil	(μ)	
A-2	x-y	3.4	6.69	0.33	(8.5)	0.50	(12.75)	9.51	(241.5)	1.5 : 1.3
	x-z	2.2	3.1	0.47	(11.81)	0.70	(17.73)	20.7	(525.5)	1.5 : 1.3
	y-z	2.1	3.2	0.43	(10.9)	0.64	(16.35)	20.0	(508.2)	unity
B-2	x-y	1.9	3.5	0.002	(13.56)	0.53	(13.56	18.4	(466.8)	1.3 : 1.1

(a) Calculated from $\bar{c} = AL/P_yM$, where A = v/o, L = length of blank frame (mm), P = total projection of features in vertical direction, and M = monitor magnification.

(b) Calculated from $d = 3/2\ \bar{c}$.

(c) Calculated from $\lambda = \frac{2d}{3f}(1 - f)$, where (f) is the volume fraction.

Potential Methods for Equating Intermetallic Densities With an EIF Size

Viewing both the NLR and Battelle results on intermetallic particles, it was possible to quantify both intermetallic frequencies of occurrence and densities. For example, Figure 2.6 shows an exceedance diagram for preparation A2 in the X-Y orientation based on the NLR data. Each of the curves represent an exceedance line for a particular size intermetallic particle. Since there were 2000 fields examined, 2000 positive occurrences correspond to 100 percent occurrence, 200 to 10 percent, 20 to 1 percent, and so on. For example, looking at all intermetallic particles, regardless of size, approximately 200 fields out of 2000 (10 percent) contained over 16 intermetallic particles; while only about 10 blocks (0.50 percent) contained over 33 intermetallic particles. The same type of curves are constructed for larger intermetallic particles and all represent nearly linear exceedance curves. A very similar pattern was also observed with preparation B2 in the same orientation, as is demonstrated in Figure 2.7.

Figures 2.6 and 2.7 showed the NLR data according to frequency of occurrence of specific numbers of inclusions of greater than a certain size. Figure 2.8 presents the same type of data in a different manner as taken from the Battelle study. Looking at the X-Y plane again of preparation A2 (as previously tabulated in Column 1 of Table 2.1), it can be seen that most of the observed intermetallics were less than 0.24 mil (6 μm) but a few as large as 2.00 mil (51 μm) were noted.

By normalizing the data taken in each study to inclusions per mm^2, it was possible to compare the NLR and Battelle results in the X-Y plane averaged between both sample preparations. This comparison is shown in Figure 2.9. Significant differences exist. Most importantly, no intermetallics above 0.63 mil (16 μm) were observed in the NLR study (as compared to intermetallics up to 2.00 mil (51 μm) in the Battelle work), and approximately 5 times the number of small inclusions, less than 0.12 mil (< 3 μm), were noted in the NLR study as in the Battelle invesitgation. These discrepancies appear to be explainable on the basis of differing resolutions of the image analyzer systems. Many particles seen as single intermetallics by the Quantimet at 180X are resolvable into separate smaller intermetallics when viewed at higher magnification.

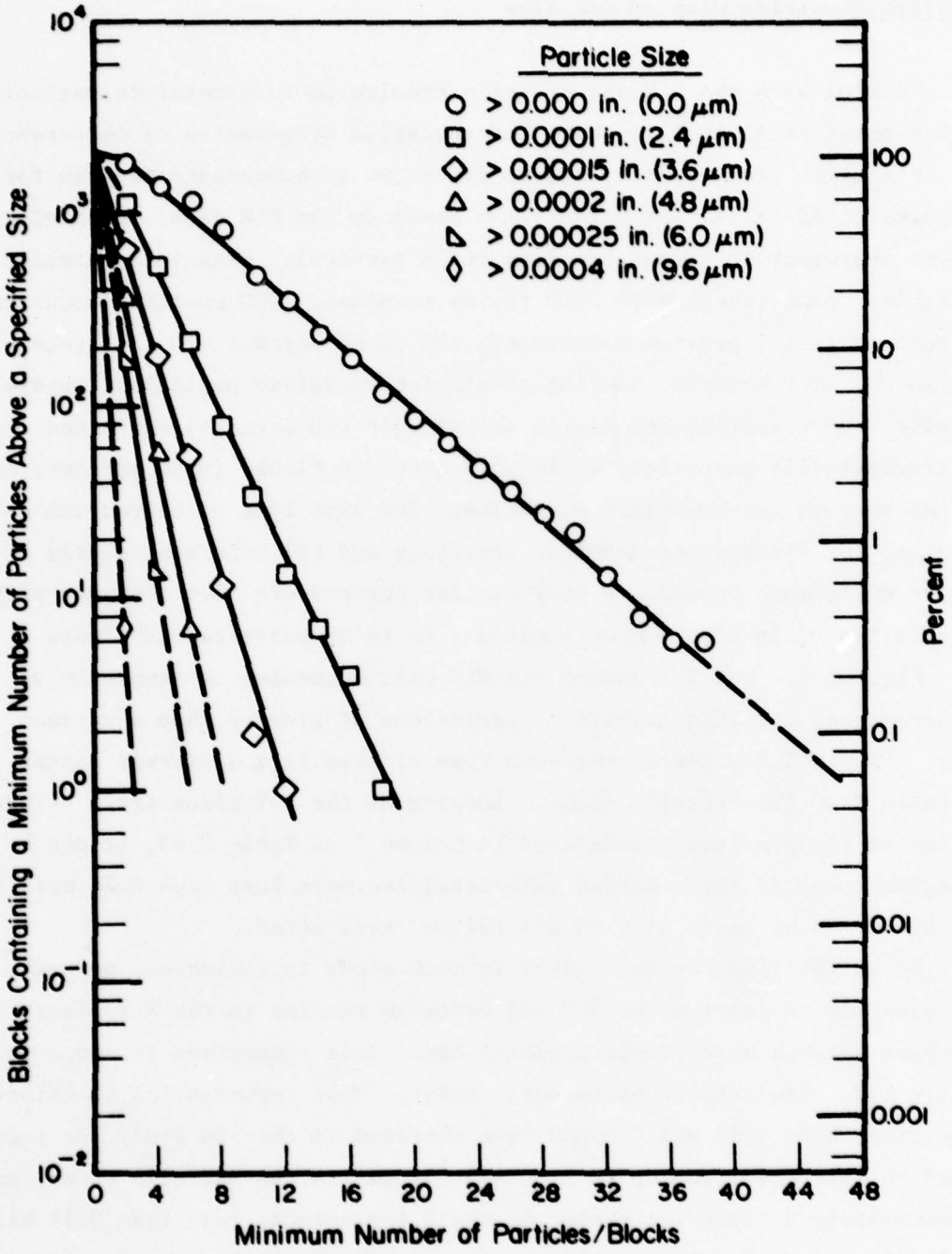

FIGURE 2.6. THE DISTRIBUTION OF INTERMETALLIC PARTICLES FOR PREPARATION A2 IN THE X-Y ORIENTATION, NLR RESULTS

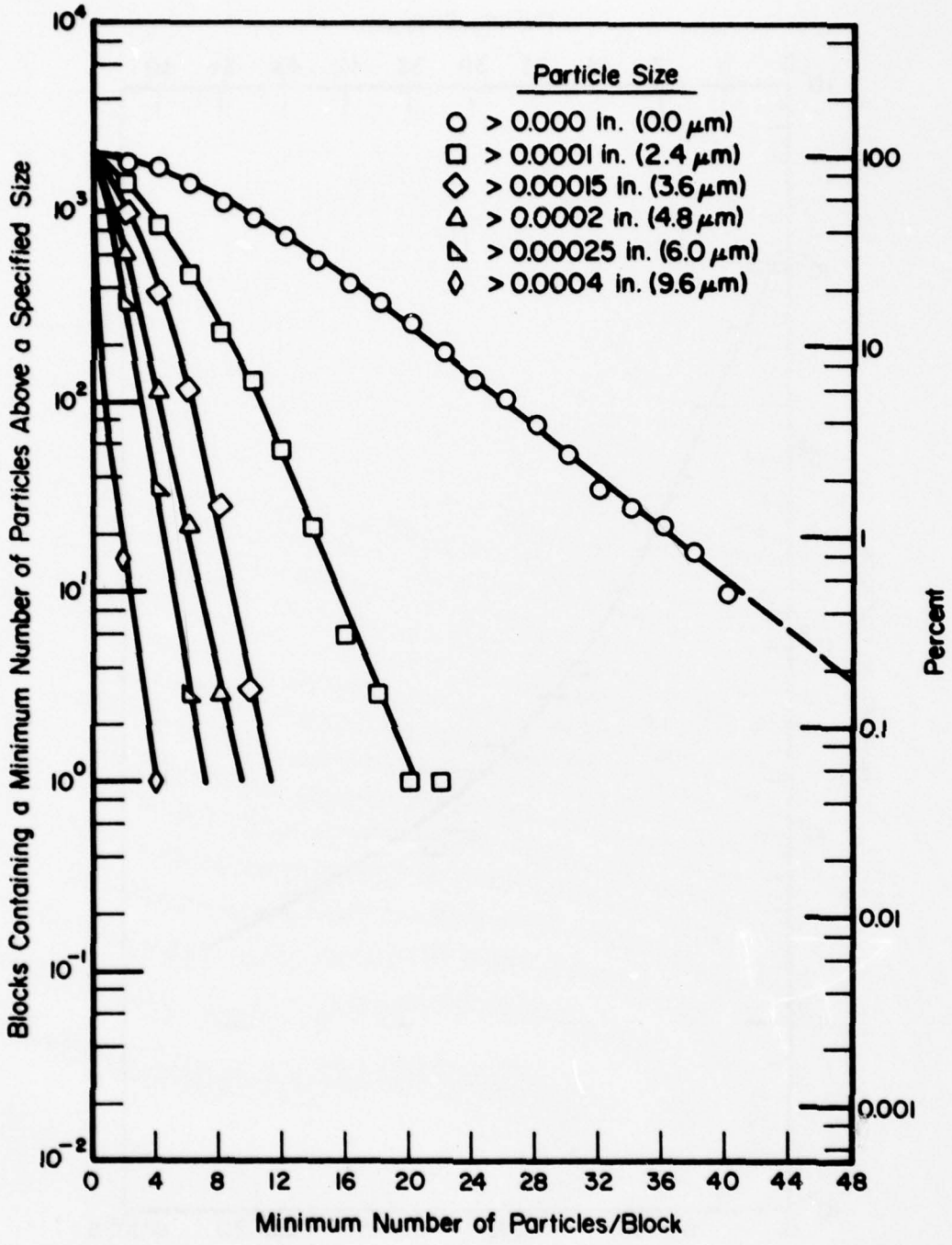

FIGURE 2.7. THE DISTRIBUTION OF INTERMETALLIC PARTICLES FOR PREPARATION B2 IN THE X-Y ORIENTATION, NLR RESULTS

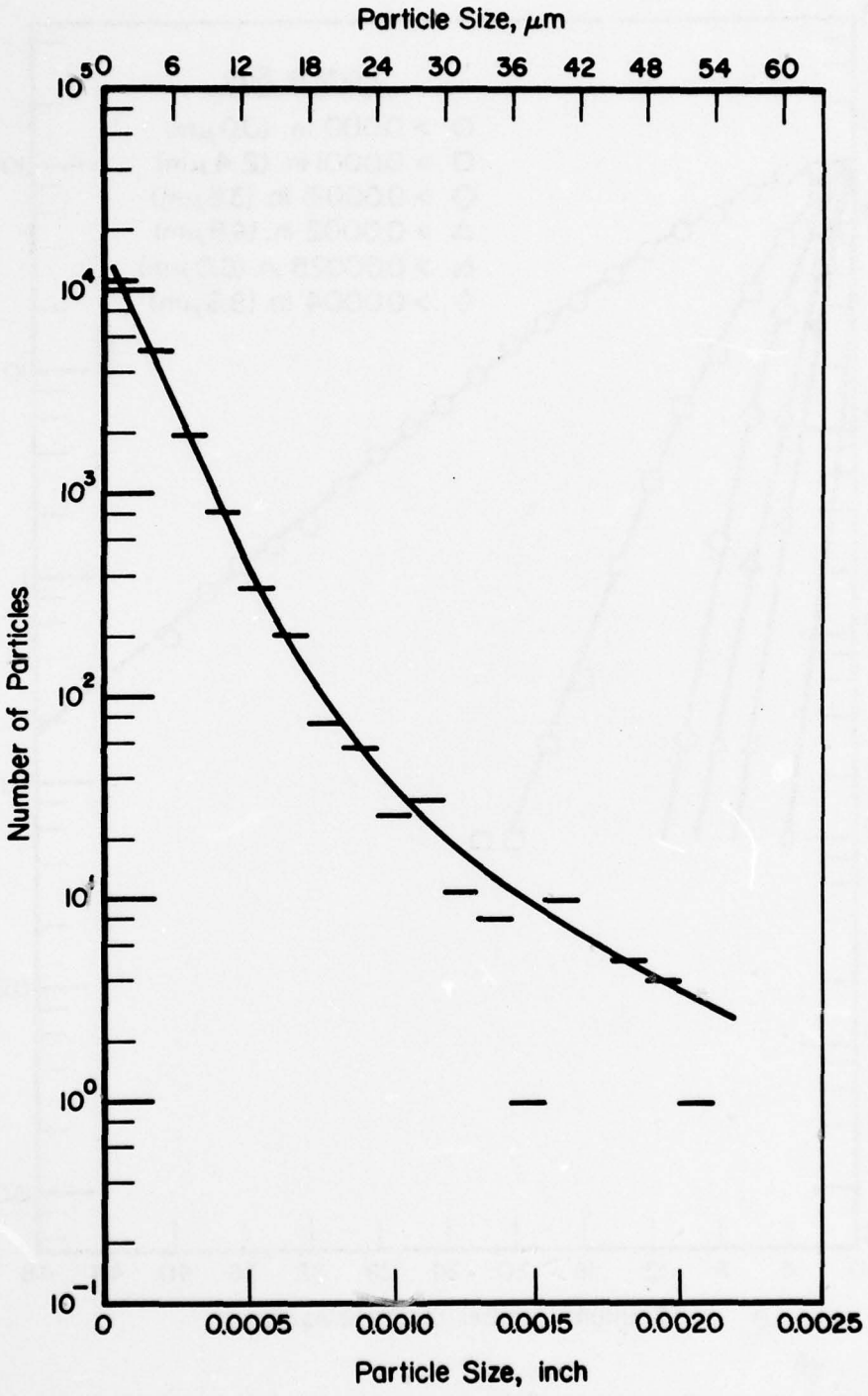

FIGURE 2.8. THE DISTRIBUTION OF INTERMETALLIC PARTICLES FOR PREPARATION A2 IN THE X-Y ORIENTATION, BATTELLE RESULTS

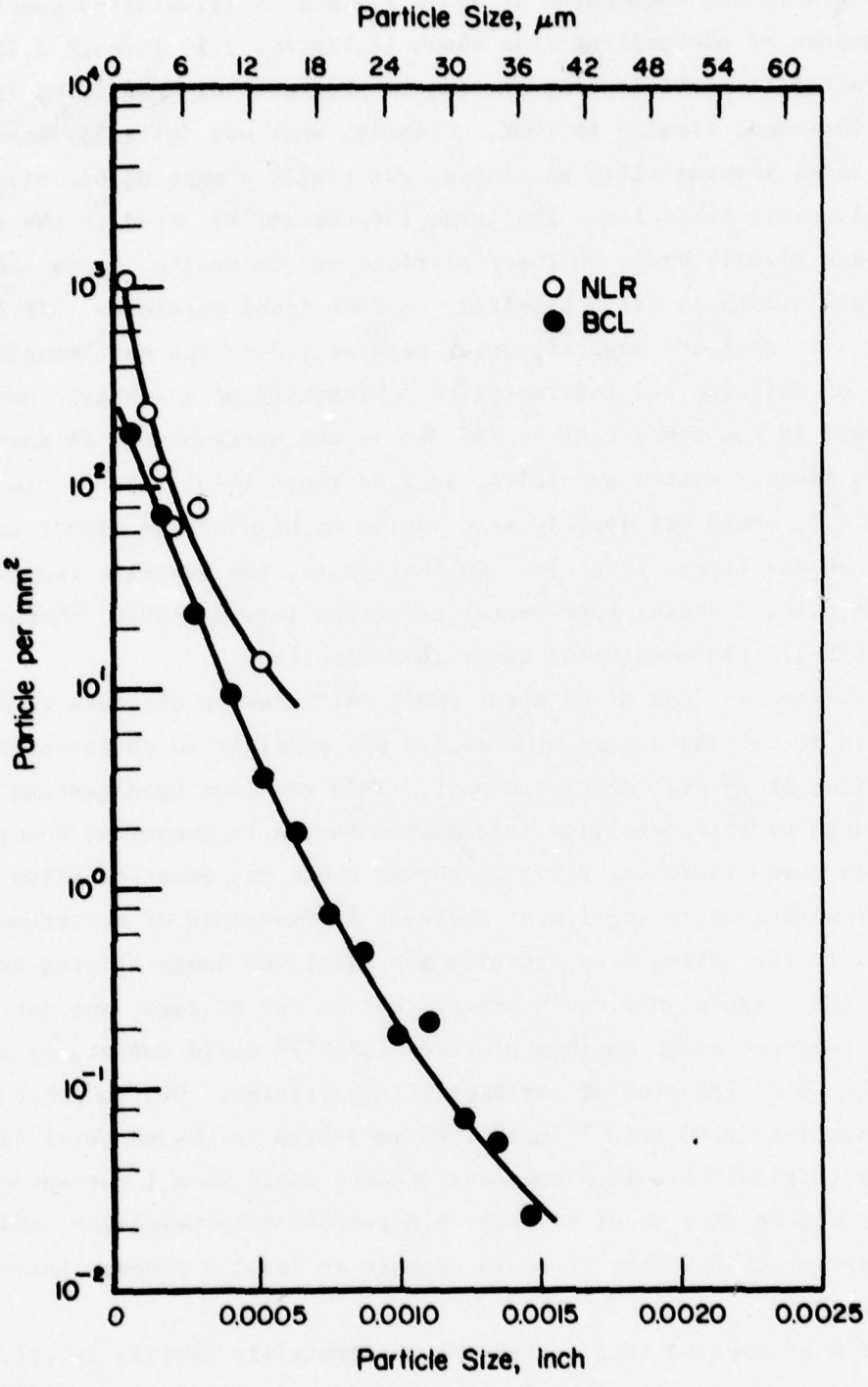

FIGURE 2.9. A COMPARISON OF BATTELLE AND NLR RESULTS ACCORDING TO NORMALIZED PARTICLE DENSITY

This was previously documented in Table 2.2 and is illustrated specifically in a sequence of photomicrographs shown in Figures 2.10 through 2.12, where an intermetallic particle congregation is progressively magnified from 180X to 390X and, finally to 700X. Clearly, what was initially seen as several large intermetallic particles, was really a mass of closely spaced, relatively small particles. The large intermetallics cited in the Battelle results are clearly based on these particle conglomerates, while the NLR results are evidently based primarily on individual particles. It is somewhat less obvious, however, which perspective is the most meaningful in terms of defining the intermetallic "character" of a specific material. When viewed in the context of an EIF, it is not unreasonable to assume that very closely spaced particles, such as those identified as clusters in Table 2.2, would act jointly at a region of high stress almost in the same way as one larger particle. On that basis, the Battelle results seemed to offer a useful representation of the intermetallic "character" of the 7075-T73 plate material under investigation.

Extending the idea of adjacent small particles or clusters working jointly in an initial damage process, it was possible to characterize the material in an even simpler manner. This was done by digesting the percent area of intermetallics information into a frequency of occurrence diagram as shown in Figure 2.13. Although there was some variation between sample preparations, a log-linear decrease in frequency of occurrence was evident with increasing area fraction per block (or image viewing area). Based on this figure, one would expect that on the average, one out of 100 randomly selected sites on this plate of 7075-T73 would contain at least a 4.8 percent area fraction of intermetallic particles. Or, in other words, given a specific 1.00×10^{-3} inch^2 (.65 mm^2) site in the material (suppose it is the critical site in a component) there would be a 1 percent chance that it would be made up of at least 4.8 percent intermetallics, and only a 0.05 percent chance that it would contain at least 8 percent intermetallics.

On the assumption that increasing intermetallic density in critical areas of a component was directly correlated to decreasing crack initiation resistance and reduced fatigue life, it was postulated that an EIF could also be tied to the size and distribution of intermetallic particles. This idea was evaluated in the experimental program which is described in the following paragraphs, beginning with the specimen design and preparation.

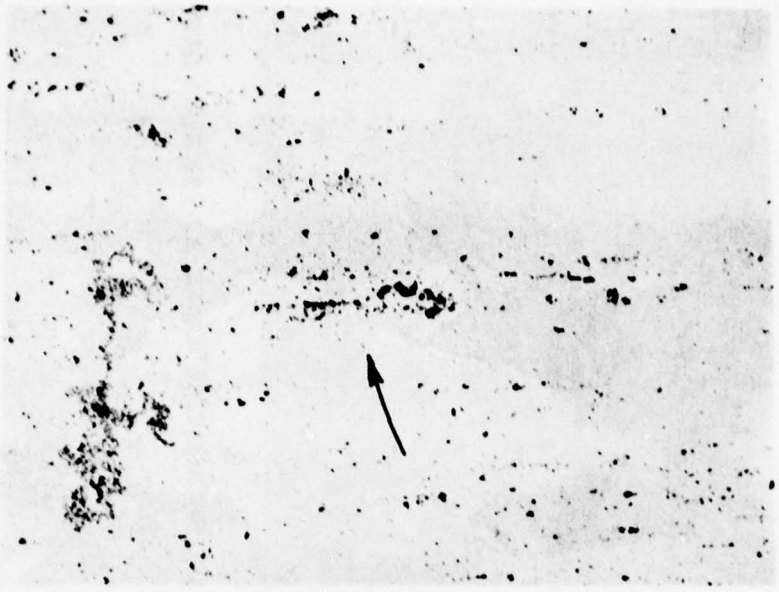

FIGURE 2.10. AN INTERMETALLIC CLUSTER (ARROW) IN PREPARATION B-2, ORIENTATION VIEWED AT 180 DIAMETERS

FIGURE 2.11. AN INTERMETALLIC CLUSTER IN PREPARATION B-2, ORIENTATION VIEWED AT 390 DIAMETERS

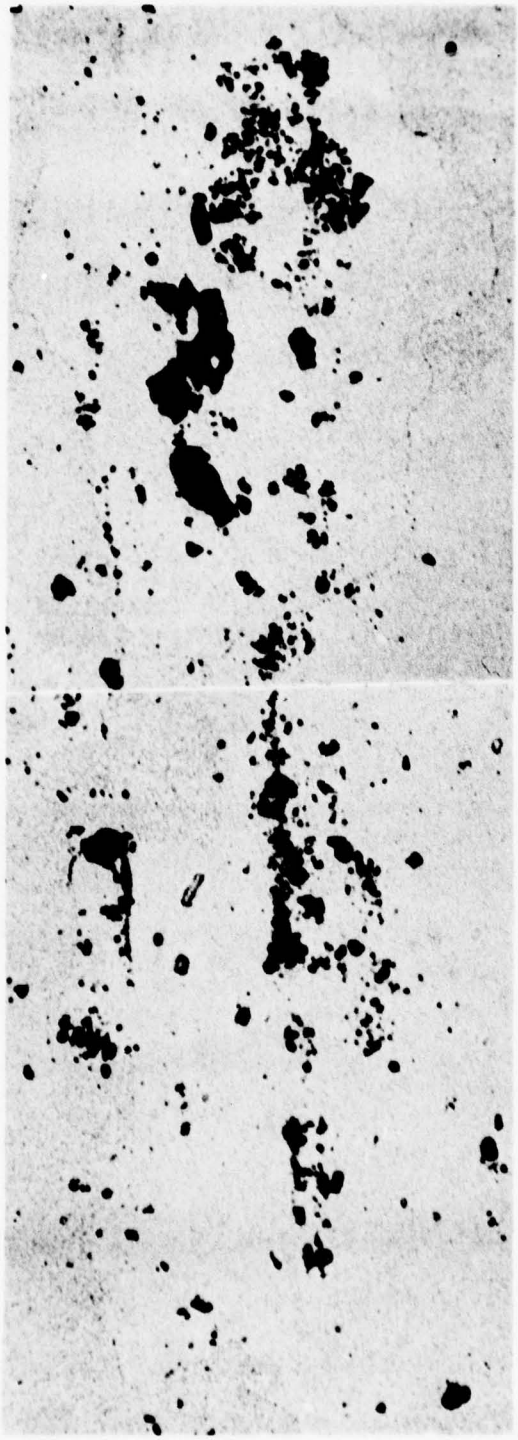

FIGURE 2.12. AN INTERMETALLIC CLUSTER IN PREPARATION B-2, X-Y ORIENTATION VIEWED AT 700 DIAMETERS

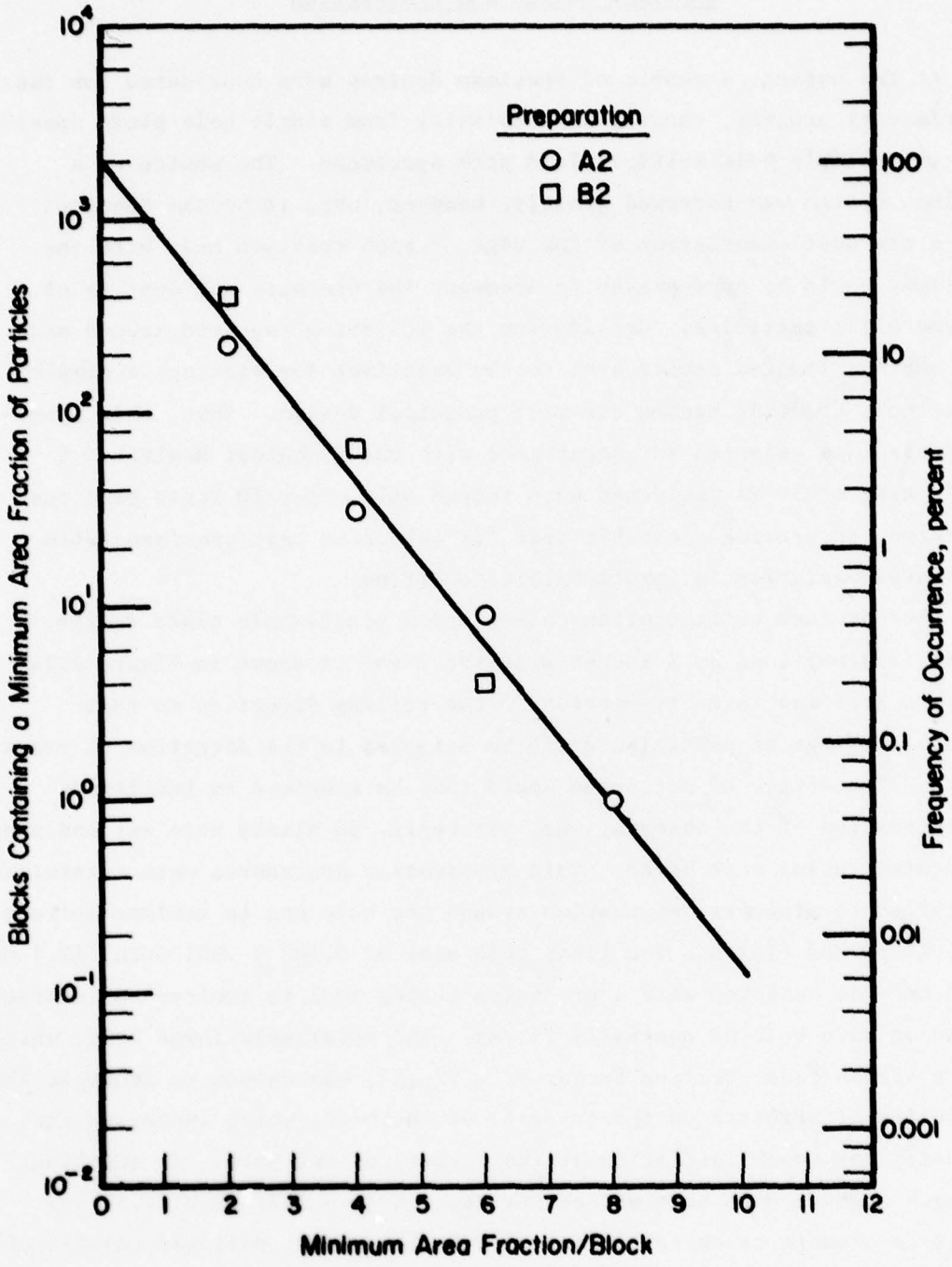

FIGURE 2.13. A FREQUENCY OF OCCURRENCE DIAGRAM ON THE VOLUME FRACTION OF INTERMETALLIC PARTICLES FOR 7075-T73 PLATE

Specimen Design and Preparation

At the outset, a number of specimen designs were considered for the experimental program, ranging in complexity from single hole plate specimens to multiple hole-multiple load path specimens. The choice of a specimen design was narrowed greatly, however, when it became apparent that a pre-test examination of the edge of each specimen hole with the Quantimet would be appropriate to document the presence and density of intermetallic particles. Considering the polishing required around each hole and the limited access area to the Quantimet for viewing, a simple, single hole specimen became the most practical design. Thus, this specimen design was selected in concurrence with the Technical Monitor. A sample size of 50 was selected even though only about 20 tests were contemplated, to provide a sizable base for selecting test specimens with the widest variation in intermetallic densities.

The specimen configuration chosen was a single-hole plate design, 9 inches (229 mm) long by 3 inches wide (76.2 mm) as shown in Figure 2.14. The specimen axis was taken transverse to the rolling direction so that eventual strings of particles would be oriented in the direction of crack growth. The effect of particles would thus be enhanced to facilitate interpretation of the observations. To begin, 50 blanks were cut and sized and central holes were bored. Hole preparation procedures were carefully controlled to minimize deformation around the hole and to achieve uniform hole sizing and finish. The final hole size of 0.500 $\pm$ .001 inch (12.7 mm $\pm$ .03 mm) was achieved with a precision boring tool to achieve an interior finish on each hole of nominally 25 rms. The relatively large hole, which gave a stress concentration factor of 2.57 [5], was chosen to decrease the biaxiality of stresses on the interior of the hole, which increased the potential for crack initiation at the corners of the hole. In addition, the back edge of each hole was corner-rounded to a 1/16-inch (1.59 mm) radius to promote crack initiation on only the front, polished corners of the hole where microscopic examinations were made.

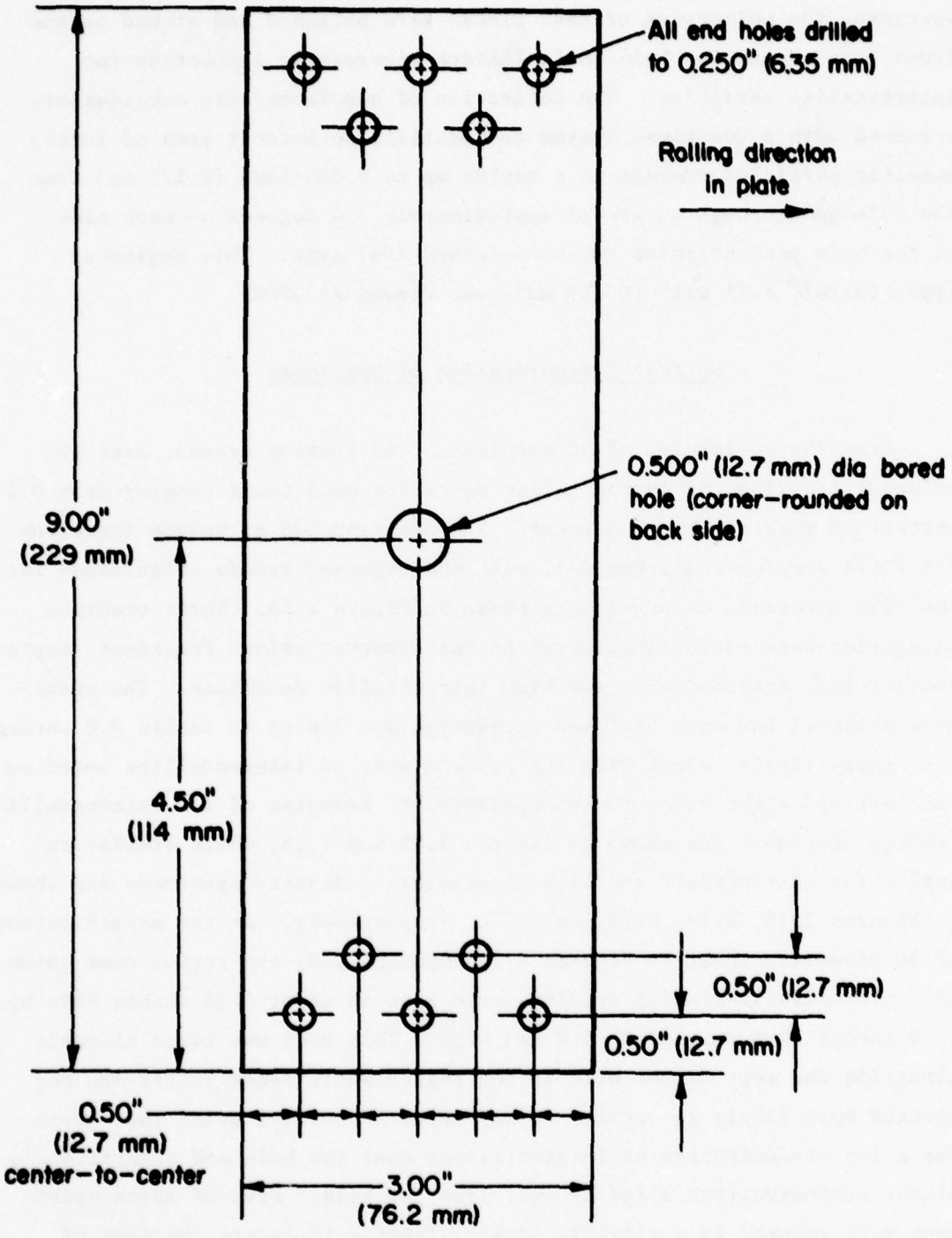

FIGURE 2.14. SPECIMEN DESIGN FOR CRACK INITIATION/INCLUSION STUDY

After the central holes were drilled and corner-rounded in each specimen, the collection of test pieces were polished and etched on the front face around the hole to facilitate microscopic inspection for intermetallic particles. The collection of specimens were subsequently screened with a Quantimet System to identify the percent area of intermetallic particles present in a region up to 0.005-inch (0.127 mm) from the hole and through an arc of approximately 3.4 degrees on each side of the hole perpendicular to the intended load axis. This region of approximately 2.59 mil^2 (0.167 mm^2) was viewed at 390X.

Optical Categorization of Specimens

From the collection of 50 specimens (100 viewing areas), area (or volume)* fractions of intermetallic particles were found ranging from 0.2 percent to greater than 4 percent. The distribution of volume fractions for these samples conformed well with the expected trends established for the bulk material, as previously shown in Figure 2.13. Three specimen categories were established based on the observed volume fractions, representing low, intermediate, and high intermetallic densities. The specimens selected for each of these categories are listed in Tables 2.4 through 2.6, respectively, along with the percent area of intermetallics noted on the left and right side of each specimen.** Examples of low intermetallic density specimens are shown in Figures 2.15 and 2.16, while similar examples for intermediate and high intermetallic density specimens are shown in Figures 2.17, 2.18, 2.19, and 2.20, respectively. At the magnification of 50 diameters shown in Figures 2.15 through 2.20, the region over which the intermetallic density readings were made is about 0.26 inches wide by 1.50 inches (0.6 mm wide by 3.8 mm) high. This area was taken directly alongside the edge of the hole in the region where crack initiation was thought most likely to occur. It was noted in several cases that there was a low concentration of intermetallics near the hole and significantly higher concentrations slightly away from the hole. Five of these specimens were rebored to a slightly larger diameter to locate the edge of the hole in the middle of the intermetallic particle cluster.

---

* On measurements including a sufficiently large number of particles, the area fraction of particles seen on the surface is statistically identical to the volume fraction of particles in the plate [6].

** Left and right were established relative to the polished surface with the etched specimen number oriented on the bottom.

TABLE 2.4. SPECIMENS SELECTED FOR CATEGORY I – LOW PARTICLE CONTENT (≤1.0 PERCENT)

Specimen Number	Percent Area Intermetallics	
	Left	Right
10	1.0	1.0
11	0.4	0.6
32	0.8	0.6
40	0.4	0.8
50	0.9	0.9
Alternates		
48	0.6	0.6
2	0.4	1.2
21	0.4	1.2
20	0.8	1.2
26	0.8	1.2

TABLE 2.5. SPECIMENS SELECTED FOR CATEGORY II – INTERMEDIATE PARTICLE CONTENT (≃2.0 PERCENT)

Specimen Number	Percent Area Intermetallics	
	Left	Right
16	2.0	1.8
18	0.8	2.0
33	1.2	2.0
34	2.0	2.0
35	1.6	2.0
Alternates		
27	0.6	1.9
37	1.2	1.9
19	1.8	1.0
39	1.6	1.8
42	1.8	1.4

TABLE 2.6. SPECIMENS SELECTED FOR CATEGORY III – HIGH PARTICLE CONTENT (>3.0 PERCENT)

Specimen Number	Percent Area Intermetallics	
	Left	Right
5	2.4	4.0
36	2.4	3.2
43	2.2	3.6
46	2.6	4.2
47	3.4	2.4
Alternates		
24	3.0	1.2
28	1.4	3.0
9	1.8	2.8
Rebores		
31[a]	2.0	2.8
17[b]	1.0	2.4

[a] Rebored hole diameter = 0.521 in.

[b] Rebored hole diameter = 0.529 in.

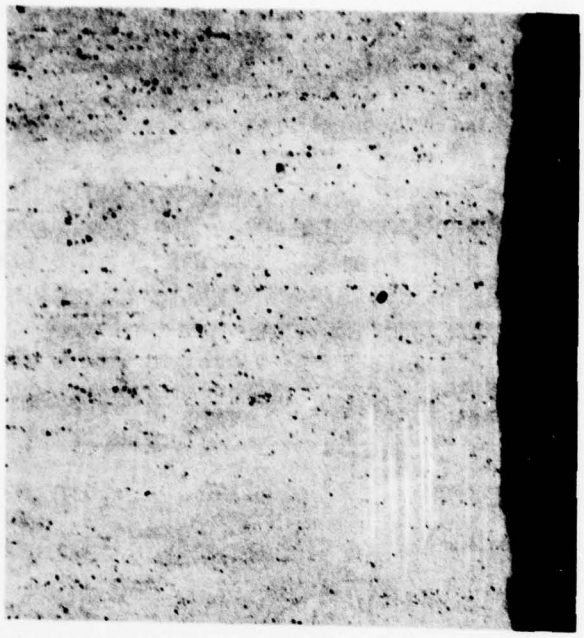

(a) Left Side of Hole, 0.4 Percent Intermetallics Near Edge

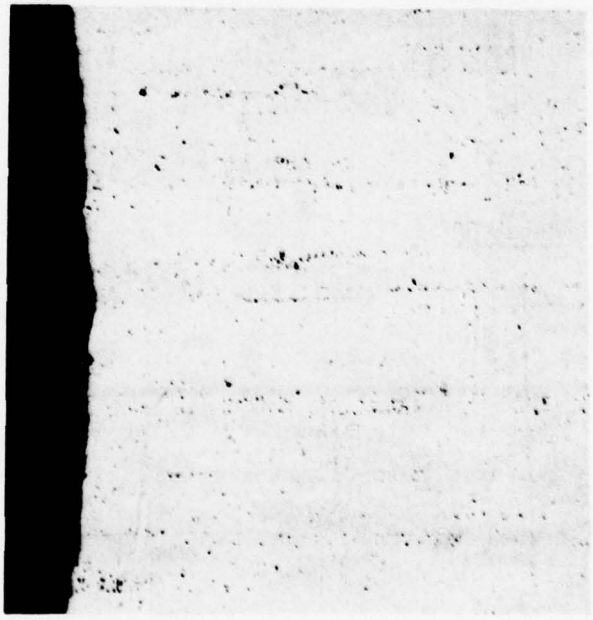

(b) Right Side of Hole, 0.6 Percent Intermetallics Near Edge

FIGURE 2.15. SPECIMEN NO. 11 VIEWED AT 50 DIAMETERS

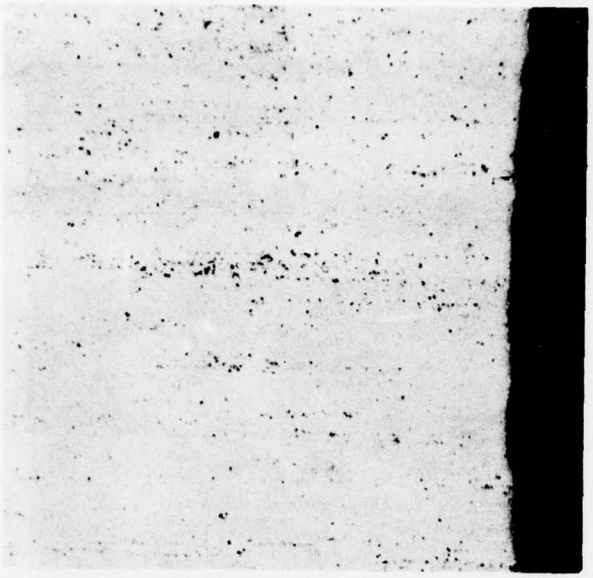

(a) Left Side of Hole, 0.8 Percent Intermetallics Near Edge

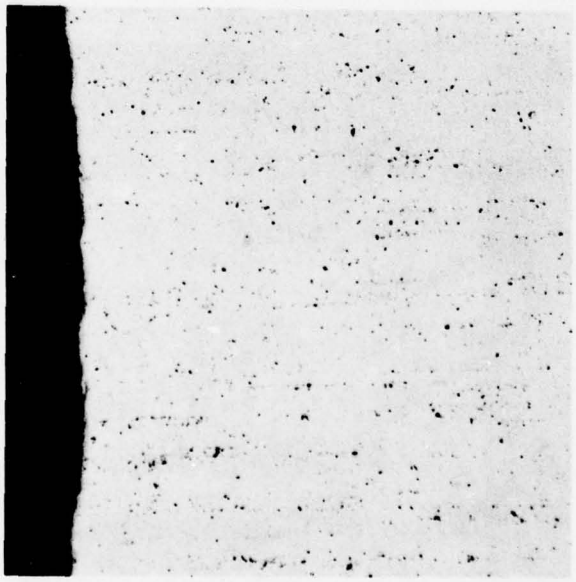

(b) Right Side of Hole, 0.6 Percent Intermetallics Near Edge

FIGURE 2.16. SPECIMEN NO. 32 VIEWED AT 50 DIAMETERS

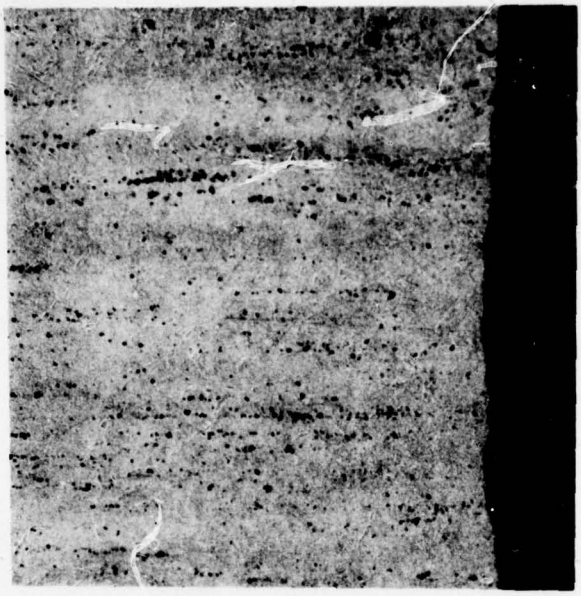

(a) Left Side of Hole, 0.8 Percent Intermetallics Near Edge

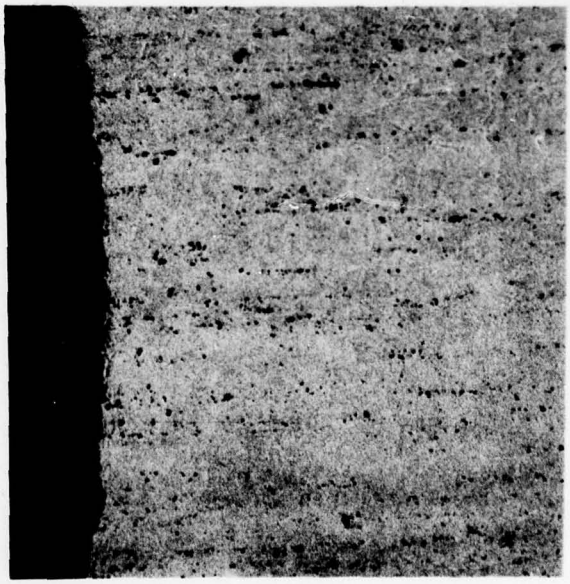

(b) Right Side of Hole, 2.0 Percent Intermetallics Near Edge

FIGURE 2.17. SPECIMEN NO. 18 VIEWED AT 50 DIAMETERS

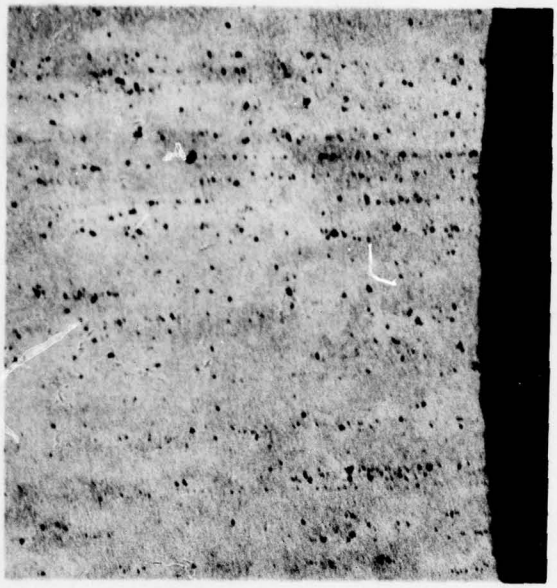

(a) Left Side of Hole, 1.2 Percent Intermetallics Near Edge

(b) Right Side of Hole, 2.0 Percent Intermetallics Near Edge

FIGURE 2.18. SPECIMEN NO. 33 VIEWED AT 50 DIAMETERS

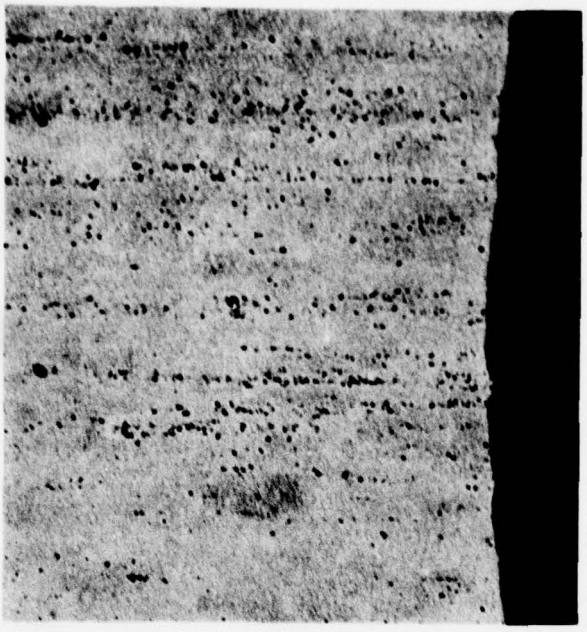

(a) Left Side of Hole, 2.4 Percent Intermetallics Near Edge

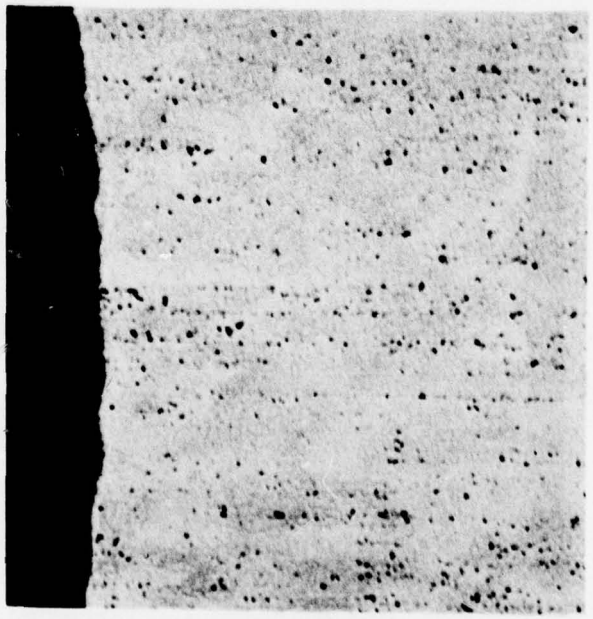

(b) Right Side of Hole, 3.2 Percent Intermetallics Near Edge

FIGURE 2.19. SPECIMEN NO. 36 VIEWED AT 50 DIAMETERS

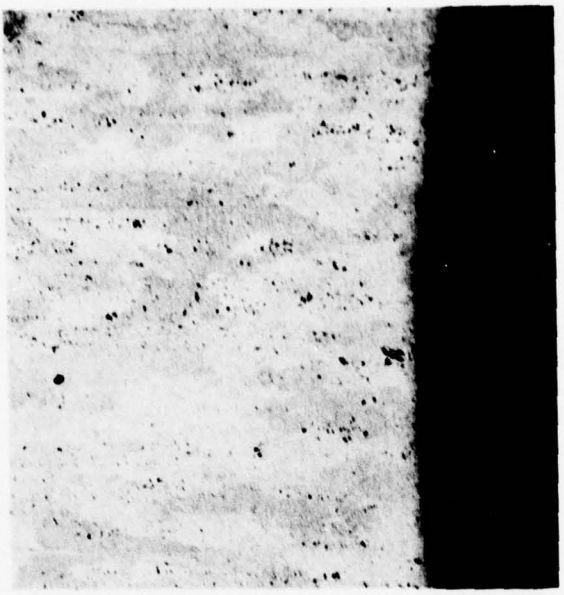

(a) Left Side of Hole, 2.4 Percent Intermetallics Near Edge

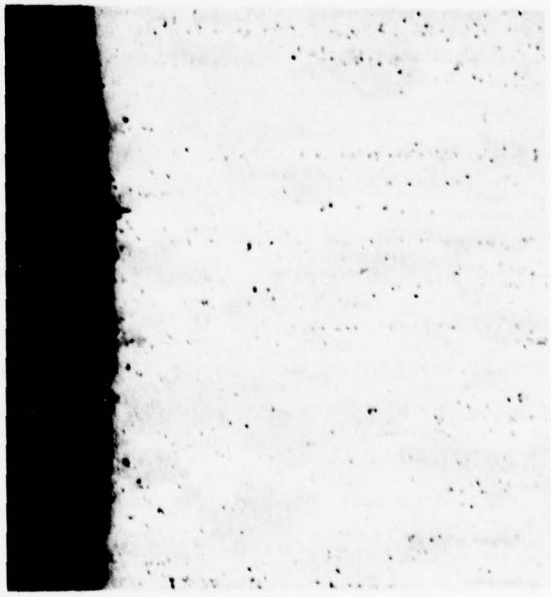

(b) Right Side of Hole, 4.0 Percent Intermetallics Near Edge

FIGURE 2.20. SPECIMEN NO. 5 VIEWED AT 50 DIAMETERS

This procedure was only marginally successful, with only two of the five showing substantial increases in intermetallic density after reboring. These specimens are identified in Table 2.6.

Experimental Program

After the specimens were machined and optically characterized, the test matrix was finalized and the experimental procedures were defined.

Test Matrix

The test matrix was designed specifically to evaluate the statistical significance of fatigue life variations between center hole specimens exhibiting low, intermediate, and high intermetallic content at the hole corners. Two different maximum stress levels of 18.0 and 15.0 ksi (124 and 103 MN/m^2) with a ratio of R = 0.05* were chosen to achieve average fatigue lives of about 50,000 cycles and 200,000 cycles. At least three tests were to be conducted for each stress level and intermetallic category which resulted in a minimum of 18 experiments.

Experimental Procedures

All experiments were conducted in a 25,000-pound (11,360 Kg) capacity, closed-loop MTS electrohydraulic test system. The specimens were cycled in load control at frequencies ranging from 10 to 20 cycles per second. Load levels were continuously monitored and controlled within 1 percent accuracy. A traveling microscope with a 20-power reticule was used to monitor both crack initiation and propagation.

The basic test procedure was to mount a selected specimen in the machine (while maintaining hole orientation with respect to optical micrographs), cycle the specimen until a crack initiated on one or both corners of the hole, remove the specimen for further optical examination, and finally, reinstall the specimen and cycle to failure while monitoring crack propagation. The size of crack constituting initiation varied somewhat from specimen to specimen depending on how quickly the crack could be observed, but most cracks were found in the range of 0.003 to 0.010 inch (0.076 to 0.25 mm).

* R – ratio of minimum/maximum stress.

Experimental Results

The experimental results are subdivided into three separate but related areas. First, the fatigue-crack initiation and cycles to failure data are presented, followed by the optical review of crack initiation sites, and lastly, the scanning electron microscope results are presented.

Fatigue-Life Data

Results of the experimental program are presented in Table 2.7 for each stress level, intermetallic category, and specimen number. The data include cycles to initiation and to complete specimen failure, along with the percent area of intermetallic particles along each side of the hole where initiation first occurred is asterisked.

Average crack initiation lives for the specimens tested at 18.0 ksi (124 MN/m^2) varied from a minimum of 43,100 cycles for Category 1 to a maximum of 132,400 for Category 3. This trend was in direct opposition to what was anticipated, i.e., the specimens with higher intermetallic percentages at the hole survived a greater number of cycles before crack initiation than did the specimens with a low percentage of intermetallics. These results are biased significantly by Test No. 5, however, which failed at a very high fatigue life. If that result is discounted (although no sound reason for exclusion has been found), the average fatigue lives vary by a considerably smaller margin. Regardless of whether Test No. 5 is included or not the original premise regarding intermetallic density and its effect on crack initiation was not born out.

The results at 15.0 ksi (103 MN/m^2) are similarly inconclusive, although there is some indication that Category 3 specimens do fail earlier than specimens with lower intermetallic content.

In general, the laboratory experiments which were performed did not support the originally projected relationship between high intermetallic density and low fatigue life. This lack of correlation is easily noted by examining the percentage of specimens that first initiated on the side of the hole with the highest intermetallic content-only 10 out of 19, or 53 percent initiated on the highest side. This percentage is easily discounted on the basis of random occurrence.

TABLE 2.7. FATIGUE CRACK INITIATION AND CYCLES TO FAILURE DATA FOR CENTER-HOLE PLATE SPECIMENS OF 7075-T73

Stress Level, ksi	Intermetallic Category	Specimen Number	Number of Cycles		Percent Area of Intermetallics Along Hole	
			Initiation	Failure	Left Side	Right Side
18.0	I	10	46,400	62,530	1.0*	1.0
		11	43,000	61,880	0.4	0.6*
		32	40,000	59,310	0.8*	0.6
		Avg.	43,100	61,240		
	II	16	39,200	52,100	2.0	1.8*
		18	44,100	50,000	0.8	2.0*
		33	54,300	66,650	1.2*	2.0
		Avg.	45,900	56,250		
	III	36	94,000	105,100	2.4*	3.2
		43	37,200	58,030	2.2*	3.6
		5	266,000	269,920	2.4*	4.0
		Avg.	132,400	144,350		
15.0	I	48	404,400	462,800	0.6*	0.6
		20	90,000	131,200	0.8*	1.2
		2	85,000	103,430	0.4*	1.2
		Avg.	193,100	232,430		
	II	27	323,800	340,970	0.6	1.9*
		35	254,000	278,000	1.6	2.0*
		19	180,000	186,190	1.8	1.0*
		Avg.	252,600	268,390		
	III	47	126,500	157,960	3.4*	2.4
		24	72,000	104,650	3.0*	1.2
		28	60,000	81,730	1.4	3.0*
		9	120,000	144,010	1.8*	2.8
		Avg.	94,600	122,090		

*Site of First Initiation

Of course, there remained the possibility that a detailed optical and electron microscope examination of these specimens, particularly those displaying low fatigue lives, might provide insight into the underlying factors causing the unexpected trends. Those results are presented in the following sections.

Optical Review of Crack Initiation Sites

As mentioned previously, once an observable crack was initiated in each fatigue sample, the specimen was removed for examination with an optical microscope. This practice was enlightening in several ways, and proved significant in understanding the overall test results.

One observation, made early in the study, was that the primary crack initiation site did not necessarily occur within a narrow arc of the hole perpendicular to the load axis. While categorizing the individual specimens as to intermetallic content, an arc of approximately 3.4 degrees on each side of the hole was included to a depth of about 0.005 inch (0.127 mm). Some specimens, such as Specimen No. 16 in Figure 2.21, exhibited crack initiation as much as 20 degrees away from the center line of the hole, well beyond the region which was characterized for intermetallic content. This did not happen in all cases, however, and could not be attributed to fixture misalignment or specimen design. The zone of characterization and the actual initiation site were, therefore, in some cases, completely unrelated, and any apparent correlation between intermetallic category and crack initiation performance would have been completely fortuitous. However, examination of the area of crack initiation indicated that no better correlation should be expected with the particle density at the actual initiation sites. This can be appreciated from some of the micrographs.

Inspection of Figure 2.21 also reveals another surprising result that correlates well with the test data. The site of initiation in this specimen was in a region apparently free of significant intermetallic particles, while no cracks formed at the clusters of sizable intermetallic stringers nearby. Of course, these are only surface observations and intermetallic clusters may have been subsurface to the actual initiation site.

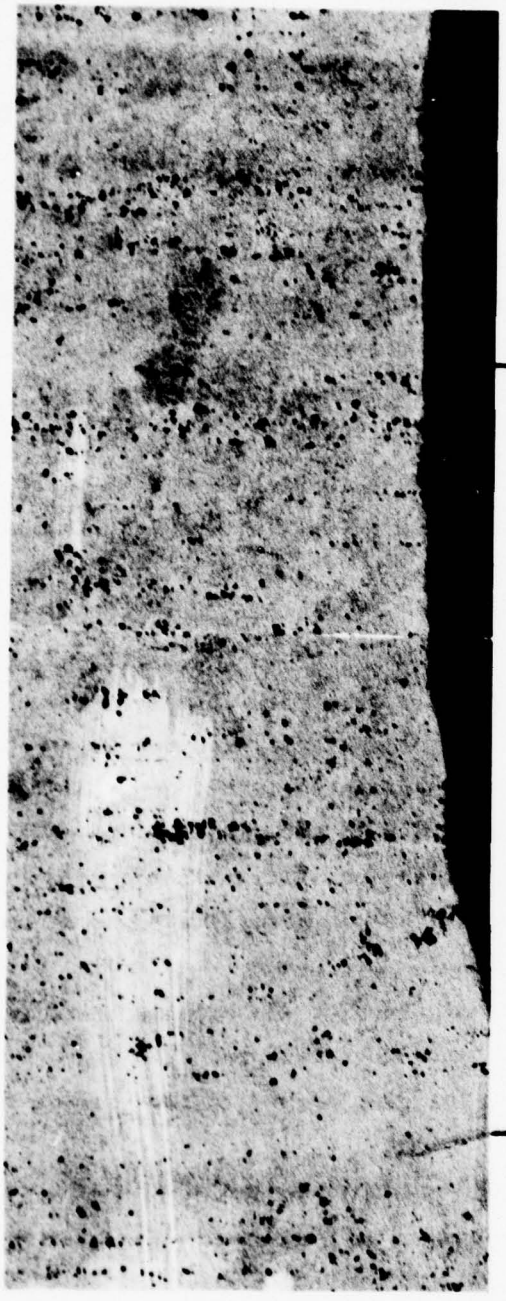

FIGURE 2.21. SPECIMEN NO. 16 VIEWED AT 50 DIAMETERS, LEFT SIDE OF HOLE WITH A CRACK INITIATED 20 DEGREES BELOW CENTER LINE OF HOLE

Some cracks did initiate at zones of significant intermetallic particles. For example, Specimens No. 27 and 28 exhibited cracks at stringers and those cracks appeared to follow along those stringers in the early stages of propagation as shown in Figures 2.22 and 2.23. These stringers are quite long in some cases (0.006 to 0.020 inch (150 to 500 μm)) compared to any recorded particles or clusters of particles. The mechanisms which lead to cracking at such stringers, while leading to a completely different crack initiation site in cases such as Specimen No. 16, remain unclear.

Multiple initiation sites were observed in several cases, as in Figures 2.24 and 2.25, but only one crack propagated beyond about 0.010 inch (0.25 mm) in every instance. The first crack to appear was not necessarily the critical one, however; in at least two instances, a small crack was observed in one area of the hole and a crack subsequently developed and lead to failure in another area on the same side of the hole.

Cracks commonly formed (five out of nine times) on both sides of the hole before the specimen failed at the 18.0 ksi (124 MN/m^2) stress range, but cracking occurred on only one side in most cases (nine out of ten times) at the lower 15.0 ksi (103 MN/m^2) stress range. This behavior is apparently attributable to the fact that the ratio of cycles to crack initiation to cycles to failure typically increases with decreasing stress for a given specimen geometry, and that the period of survival beyond crack initiation was so brief in most cases at the low stress range that the statistically expected crack on the opposite side of the hole did not have time to form.

Scanning Electron Microscope Review of Fracture Surfaces

After the specimens were failed a postmortem examination of the fracture surfaces was conducted with an ISI-100 scanning electron microscope. This work was done to confirm the point of initiation and to identify intermetallics and other irregularities which influenced the crack initiation and propagation process.

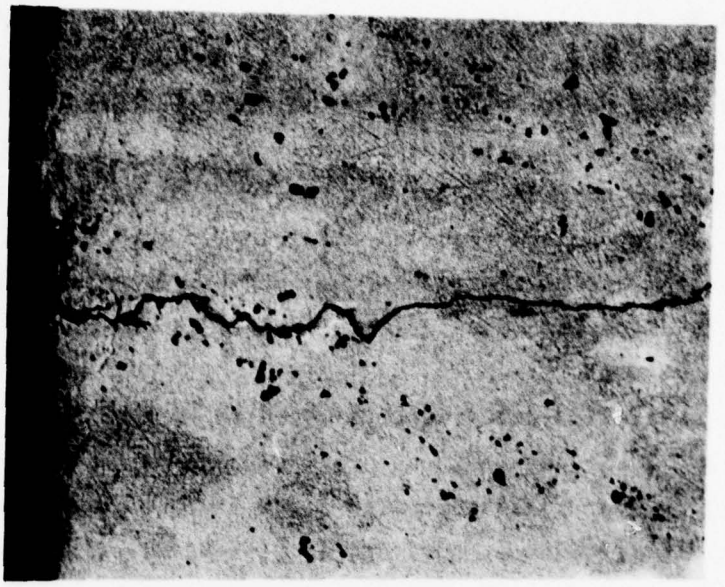

(a) Crack Initiation Zone

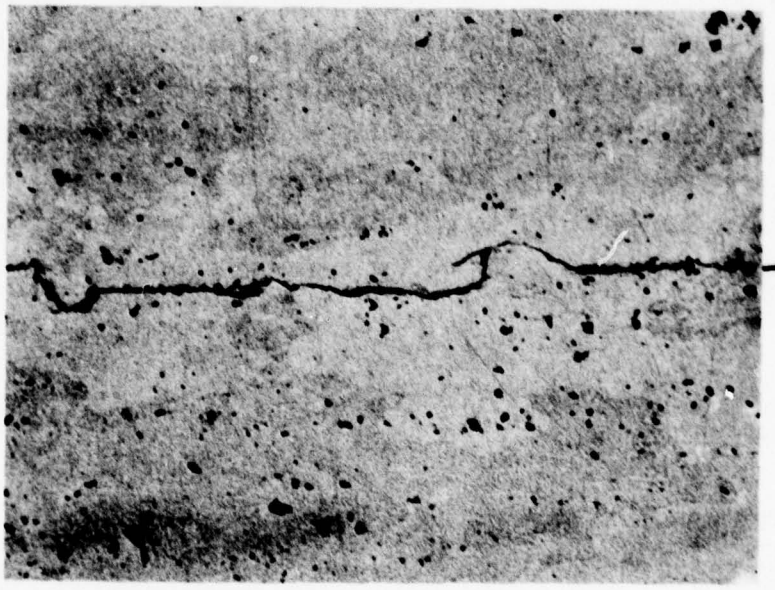

(b) Crack Propagation Zone

FIGURE 2.22. SPECIMEN NO. 27 VIEWED AT 250 DIAMETERS, RIGHT SIDE OF HOLE WITH A CRACK PASSING THROUGH INTERMETALLIC CLUSTER

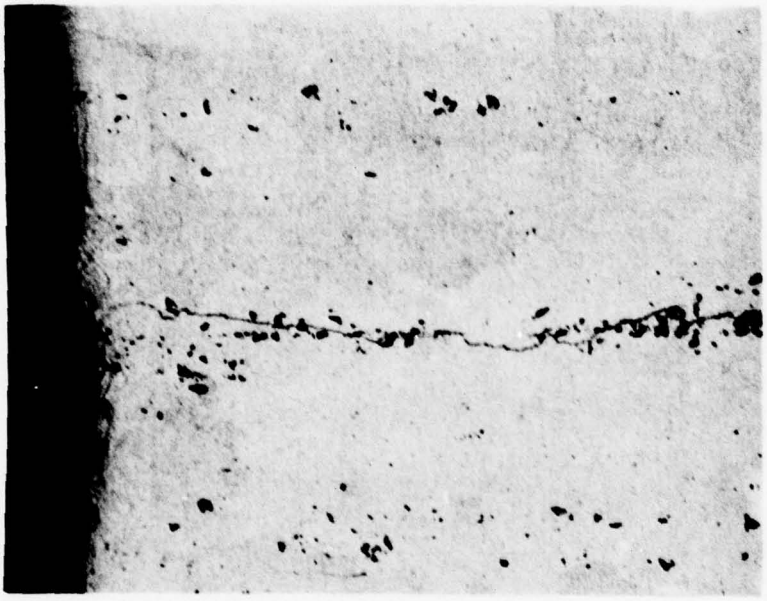

FIGURE 2.23. SPECIMEN NO. 28 VIEWED AT 200 DIAMETERS, RIGHT SIDE OF HOLE WITH A CRACK PASSING THROUGH INTERMETALLIC CLUSTER

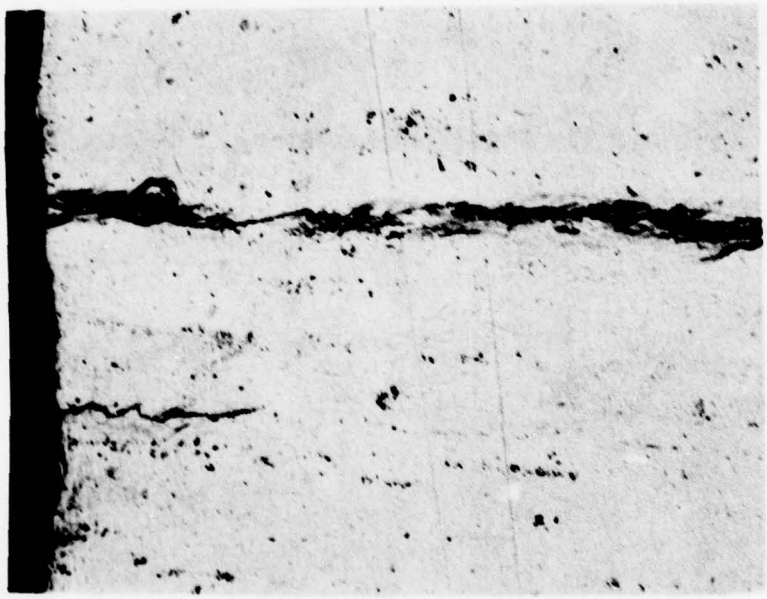

FIGURE 2.24. SPECIMEN NO. 18 VIEWED AT 100 DIAMETERS, RIGHT SIDE OF HOLE WITH MULTIPLE CRACKS FORMED

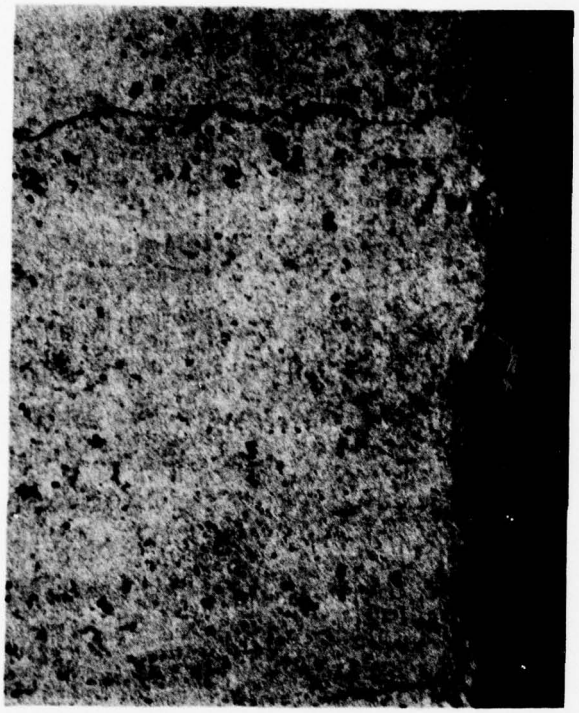

FIGURE 2.25. SPECIMEN NO. 32 VIEWED AT 250 DIAMETERS, LEFT SIDE OF HOLE WITH MULTIPLE CRACKS FORMED

It was confirmed through SEM examinations that crack initiation did occur at the corners of the hole and not interior to it. Figure 2.26 illustrates a typical fracture surface (Specimen No. 33) at low magnification. Sites of specific interest are noted on the fracture surface for future reference. Figure 2.27 shows the same fracture surface at 100X magnification, where signs of cleavage fracture become evident. A further increase in magnification to 500X in Figure 2.28 reveals the slanted initiation zone (evidently along slip lines) that was typical of nearly all the fractures. This zone was typically about 0.0005 to 0.0010 inch (12.7 to 25.4 μm) deep and triangular in shape. A close examination of this initiation zone (at 3000X, see Figure 2.28) did not reveal large intermetallic particles within it. This absence of dominant particles in the initiation zone was typical of other specimens examined also; for example, Specimens No. 24 and 16 shown in Figures 2.30 and 2.31. Intermetallics are visible in some of these photomicrographs, however, and they are comparable in size to those seen on the surface. For example, in Figure 2.31 (Specimen 16) there is a particle evident on the fracture surface that is about 0.1 mil (2.5 μm) in diameter. It is an order of magnitude smaller than the slant fracture zone preceding it, however, and it appears unlikely that it caused the crack to start. It is true that Specimen 16 did have a very short crack initiation life (39,200 cycles at 18 ksi (124 MN/m^2), but it is also true that other comparable specimens such as Specimen No. 36 displayed equally large particles in the initiation zone (See Figure 2.32) and yet, a substantially higher fatigue life – 94,000 cycles at 18 ksi (124 MN/m^2. The influence of these intermetallic particles on the crack initiation process is, therefore, rather unclear.

Once the crack propagates substantially beyond the initiation zone the role of intermetallic particles, in controlling gross crack-growth behavior at least, appears to decrease even further. Looking at zone A8 (in Figure 2.33) of previously sited Figure 2.26, it is possible to observe clearly defined striations spaced about 5×10^{-6} to 1×10^{-5} inch (.12 to .25 μm). This compares reasonably well with the macroscopic crack-growth rates seen at crack lengths of about 0.09 inch (2.2 mm) in specimens tested at a stress range of 18 ksi (124 MN/m^2).

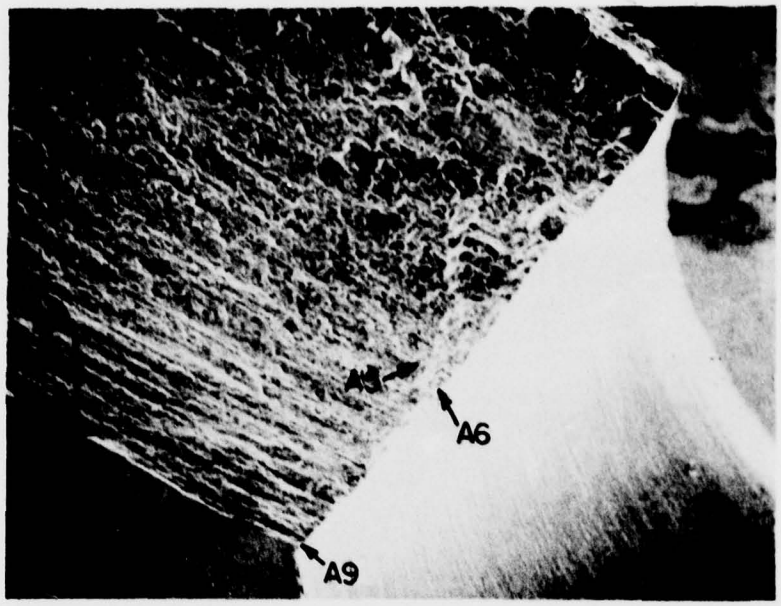

FIGURE 2.26. SPECIMEN NO. 33 VIEWED AT 17 DIAMETERS WITH THE SEM, LEFT SIDE OF HOLE

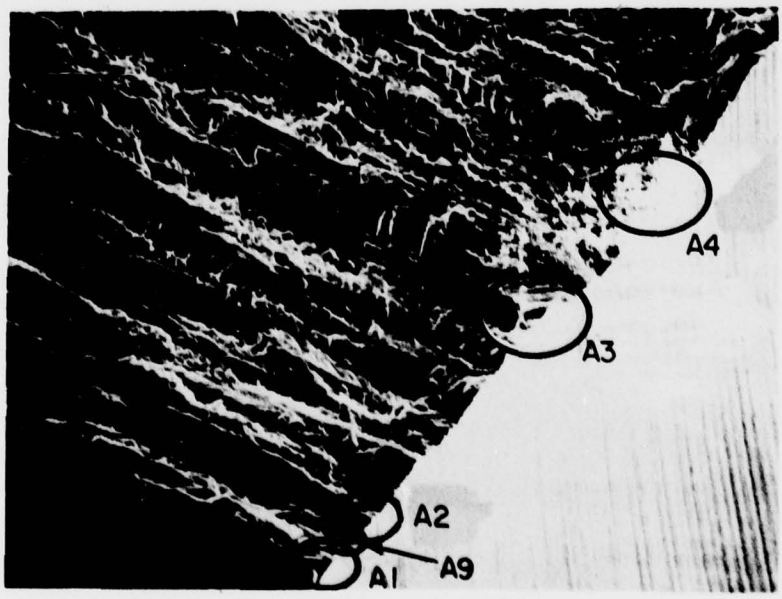

FIGURE 2.27. SPECIMEN NO. 33 VIEWED AT 100 DIAMETERS WITH THE SEM, CRACK INITIATION ZONE

FIGURE 2.28. SPECIMEN NO. 33 VIEWED AT 500 DIAMETERS WITH THE SEM, CRACK INITIATION ZONE

FIGURE 2.29. SPECIMEN NO. 33 VIEWED AT 3000 DIAMETERS WITH THE SEM, CRACK INITIATION ZONE

FIGURE 2.30. SPECIMEN NO. 24 VIEWED AT 4100 DIAMETERS WITH THE SEM, LEFT SIDE OF HOLE IN CRACK INITIATION ZONE

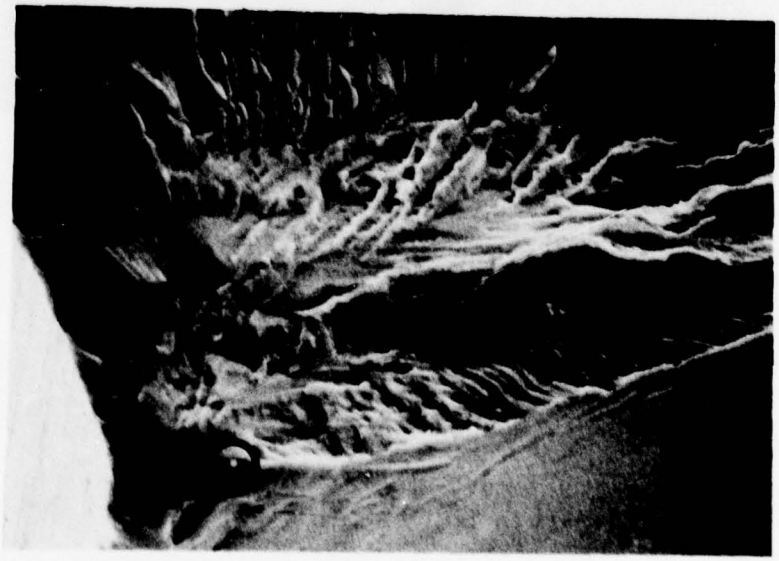

FIGURE 2.31. SPECIMEN NO. 16 VIEWED AT 500 DIAMETERS WITH THE SEM, RIGHT SIDE OF HOLE IN CRACK INITIATION ZONE

FIGURE 2.32. SPECIMEN NO. 36 VIEWED AT 500 DIAMETERS WITH THE SEM, LEFT SIDE OF HOLE IN CRACK INITIATION ZONE

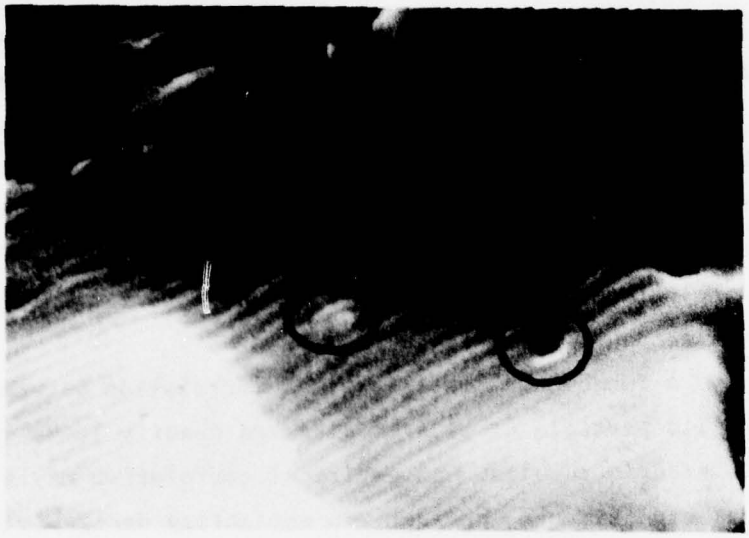

FIGURE 2.33. SPECIMEN NO. 33 VIEWED IN AREA A-8 AT 10,100 DIAMETERS WITH THE SEM SHOWING STRIATION FORMATION AND INTERMETALLIC PARTICLES

FIGURE 2.34. SPECIMEN NO. 33 VIEWED IN AREA A-7 AT 5200 DIAMETERS WITH THE SEM SHOWING STRIATION FORMATION AND INTERMETALLIC PARTICLES

Small intermetallics [about 1.2×10^{-5} inch (.31 μm)] are evident both in the surface and removed from it but they do not modify the overall striation patterns. An examination of zone A6 (Figure 2.34) of previously sited Figure 2.26 also reveals substantial striation formation along the edge of the hole (white area in lower right corner) and small intermetallics evident in the surface do not alter growth patterns here either.

A number of other SEM photographs were made, but most reflect the same basic conclusions regarding the effects of intermetallics on crack initiation and propagation.

Obviously, a fundamental metallurgical correlation between an EIF and intermetallic particle or cluster size and density looks questionable based on this study's results. An empirical correlation may still be of some practical significance, however, in estimating damage tolerance. The meaning of an empirical EIF in relation to the results of this study are discussed in the following section.

3. THE EQUIVALENT INITIAL FLAW

Calculated Initial Flaws for Fatigue Specimens

Equivalent initial flaws (EIF) for the fatigue specimens were calculated using the procedure illustrated in Figure 3.1. The test results are schematically shown in Figure 3.1(a), where the solid lines represent the measured crack-growth data and the dashed lines the extrapolation to the beginning of the life. The intercept with the ordinate ($N = 0$) then gives the equivalent initial flaw size. Since this procedure would not show how much variation in crack growth occurred, a separate crack-growth calculation for each specimen might be needed. Therefore, it has advantage to use the plot of Figure 3.1(b) where the ends of all crack-growth curves are taken together and the number of cycles is plotted reversely, i.e., as the number of cycles before fracture. If the measured crack-growth curves show little scatter, a single extrapolation is sufficient. Taking the observed total lives (N_1 through N_4 in Figure 3.1) then permits determination of the variability δ of the EIF. Obviously, it would be more logical to reverse the plot as shown in Figure 3.1(c).

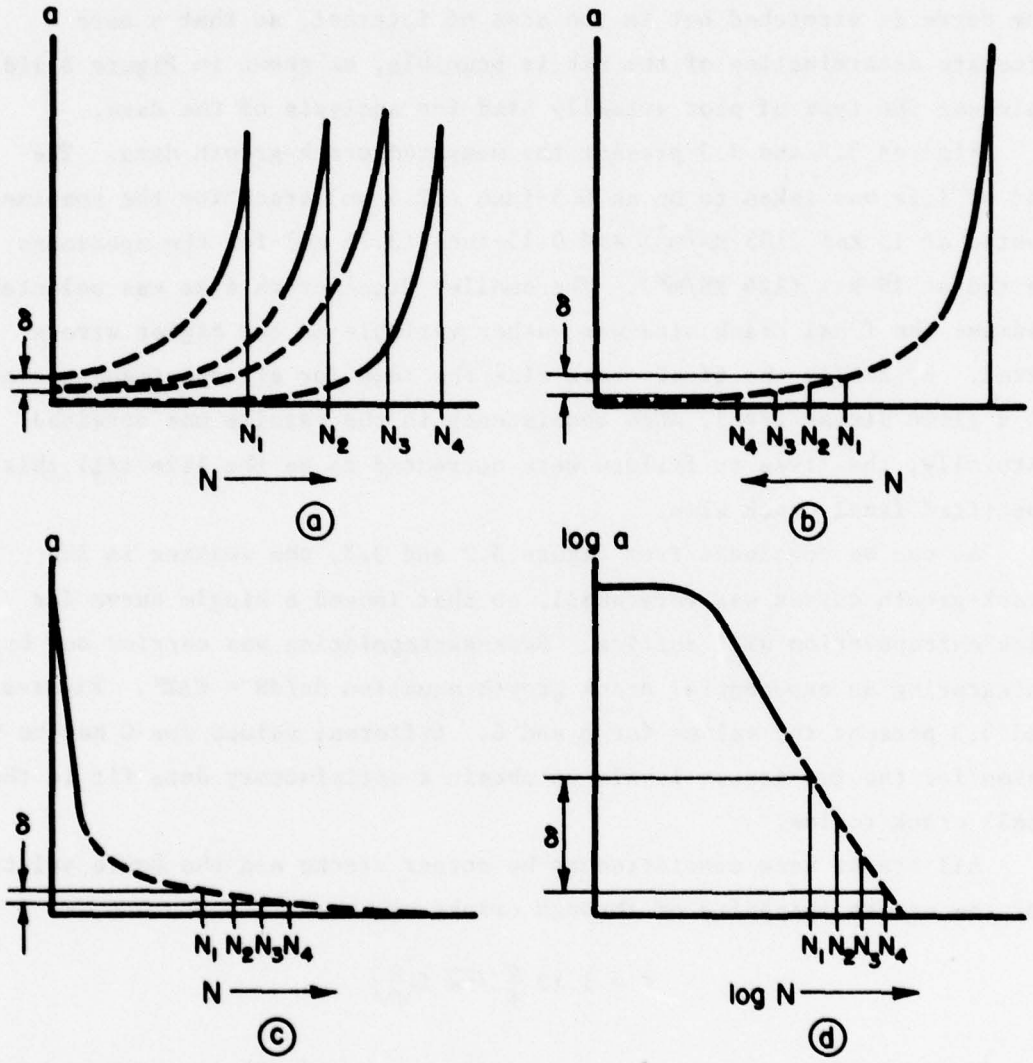

FIGURE 3.1. DETERMINATION OF THE EIF

As the crack-growth curve has an extremely small slope in the small crack regime, the variability of the EIF would not be easy to determine. Therefore, it is preferable to use a plot of log a versus log N. Where the curve is stretched out in the area of interest, so that a more accurate determination of the EIF is possible, as shown in Figure 3.1(d). This was the type of plot actually used for analysis of the data.

Figures 3.2 and 3.3 present the measured crack-growth data. The end of life was taken to be an 0.5-inch (12.5 mm) crack for the specimens tested at 15 ksi (103 MN/m^2) and 0.15-inch (3.75 mm) for the specimens tested at 18 ksi (124 MN/m^2). The smaller final crack size was selected, because the final crack size was rather variable at the higher stress level. By taking the final crack size the same for all specimens tested at a given stress level, more consistency in the results was obtained. Naturally, the lives to failure were corrected to be the life till this specified final crack size.

As can be concluded from Figure 3.2 and 3.3, the scatter in the crack-growth curves was very small, so that indeed a single curve for back-extrapolation will suffice. Back-extrapolation was carried out by integrating an exponential crack growth equation $da/dN = C\Delta K^n$. Figures 3.2 and 3.3 present the values for n and C. Different values for C had to be taken for the two stress levels to obtain a satisfactory data fit in the small crack regime.

All cracks were considered to be corner cracks and the Bowie solution for the stress intensity of through cracks was used

$$K = 1.12 \frac{\sigma}{\phi} \sqrt{\pi a}\ f\left(\frac{a}{D}\right) \quad .$$

The factor $1.12/\phi$ accounts for the corner crack; f(a/D) is the Bowie function. It was shown by Grandt [7] that the Bowie function can be represented with good accuracy by

$$f\left(\frac{a}{D}\right) = \frac{C_1}{C_2 + a/D} + C_3$$

C_1, C_2 and C_3 are numerical constants, but they have different values for the asymmetric case with one crack and the symmetric case with two cracks (one at each side of the hole):

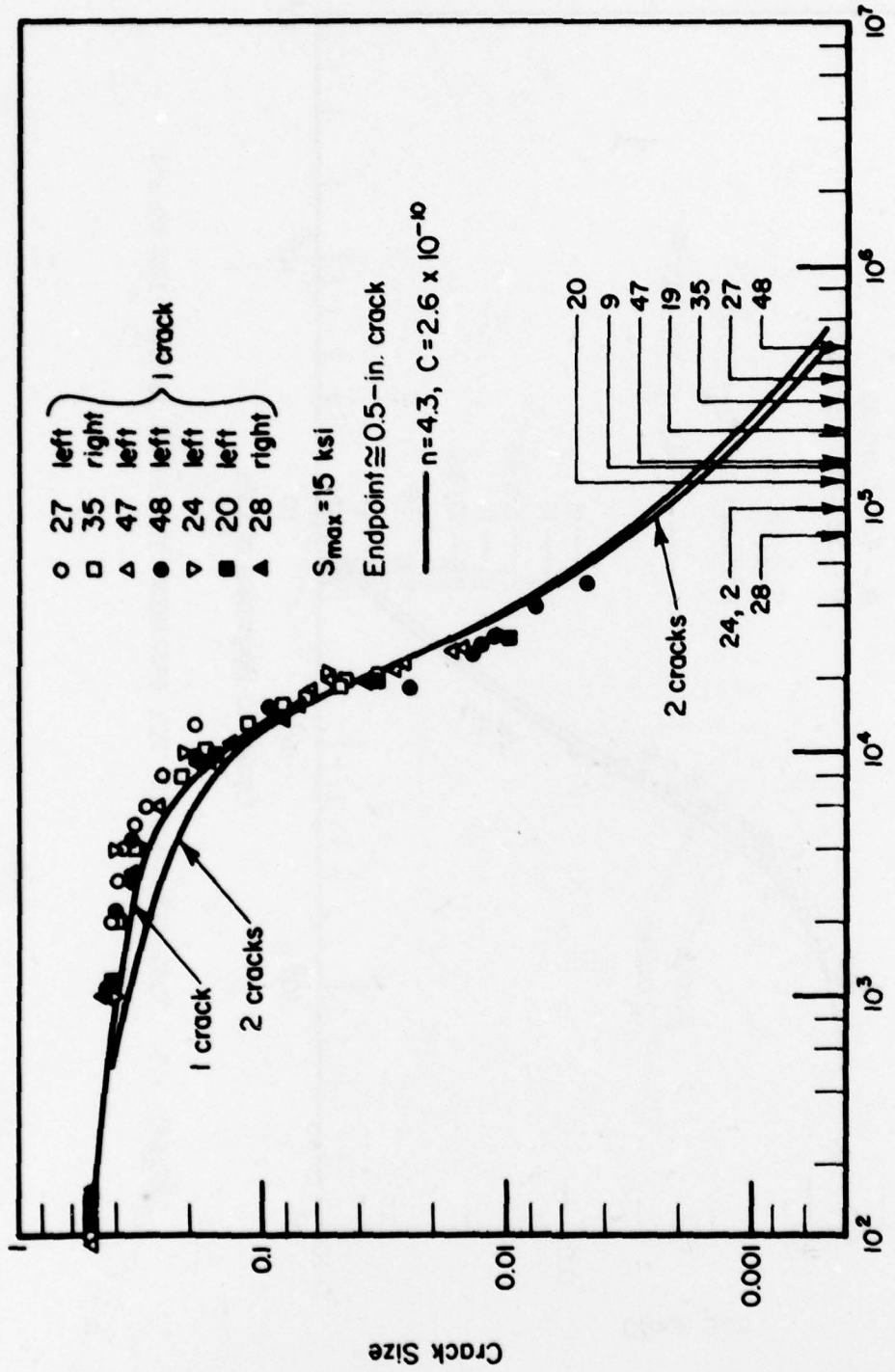

FIGURE 3.2. TEST DATA AND EIF FOR SPECIMENS TESTED AT 15 KSI (103 MN/m^2)

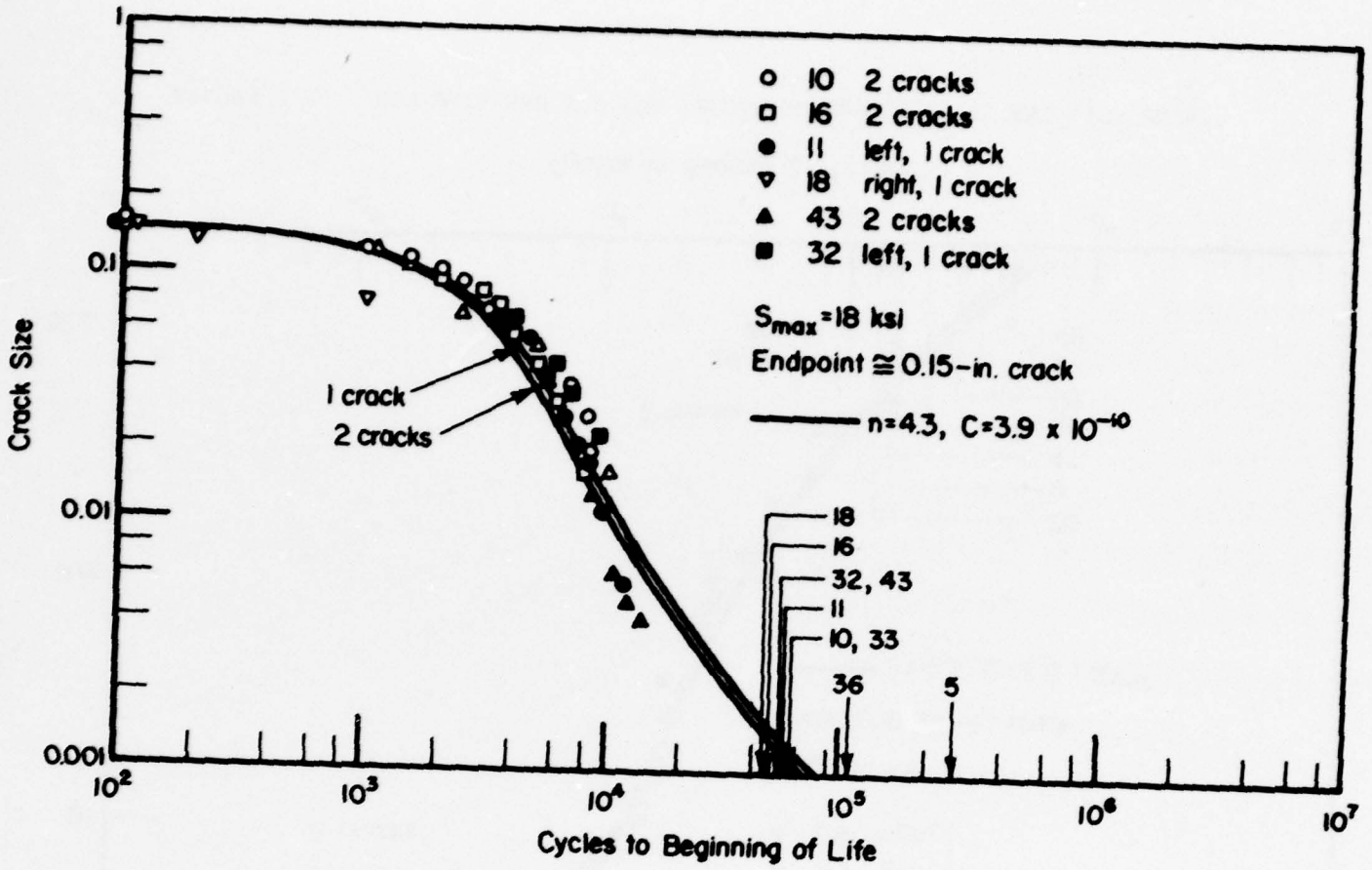

FIGURE 3.3. TEST DATA AND EIF FOR SPECIMENS TESTED AT 18 KSI (124 MN/m^2)

$C_1 = 0.4367$ for one crack, $C_1 = 0.3433$ for two cracks
$C_2 = 0.1623$ " " " , $C_2 = 0.1386$ " " "
$C_3 = 0.6762$ " " " , $C_3 = 0.9439$ " " "

The above values were used in the crack growth calculations.

The crack-growth equation was adjusted to give the best fit to the measured test data over (1) the entire range and (2) in the regime of small cracks. The calculated curves show that these two criteria could not be completely satisfied simulataneously, however, a reasonable fit was obtained.

The numbered arrows indicate the total lives of the specimens (by specimen number). A vertical section through the curves then provides the equivalent initial flaw. As can be seen from the figures, the EIF varied from 0.0005-inch to 0.0036-inch (12 to 90 μm). The individual results are compiled in Table 3.1.

It turns out that the variability of EIF is greater for the lower stress level. This is in accordance with the larger scatter in fatigue life (usually) observed at lower stress amplitudes. This by itself seems to indicate that the scatter in fatigue life in general cannot be explained on the basis of variable initial defect size, since specimens will have the same initial defect distribution whether tested at high stress or low stress.

The EIF tends to be substantially larger than the intermetallic particle parameters, but the difference is less than an order of magnitude. In recent work on the evaluation of hole quality [8], the EIF size was found to be of the order of 0.0005 to 0.005 inch, results very similar to those reported here.

Statistical Analysis of EIF

Table 3.1 presents the calculated equivalent initial flaws for all of the specimens, along with the respective fatigue lives. Considerable variation is evident in the computed EIF values, ranging over nearly an order of magnitude. The statistical significance of this variation can best be seen if the EIF values are ranked according to their logarithmic magnitude and plotted on probability paper as in Figure 3.4. Even though

TABLE 3.1. CALCULATED EQUIVALENT INITIAL FLAWS

Maximum Stress, ksi (MN/m^2)	Specimen Number	Life X 10^3	EIF		Percent, Area of Intermetallics
			Microns	Inches	
15.0 (103)	28	81.7	90	0.0036	3.0
	2	103.4	63	0.0025	0.4
	24	104.6	61	0.0024	3.0
	20	131.2	48	0.0019	0.8
	9	144.0	43	0.0017	1.8
	47	158.0	35	0.0014	3.4
	19	186.2	28	0.0011	1.0
	35	278.0	20	0.0008	2.0
	27	341.0	18	0.0007	1.9
	48	462.8	15	0.0006	0.6
18.0 (124)	18	50.0	45	0.0018	2.0
	16	52.1	40	0.0016	1.8
	32	59.3	35	0.0014	0.8
	43	58.0	33	0.0013	2.2
	11	61.9	33	0.0013	0.6
	10	62.5	33	0.0013	1.0
	33	66.6	33	0.0013	1.2
	36	105.1	23	0.0009	2.4
	5	269.9	13	0.0005	2.4

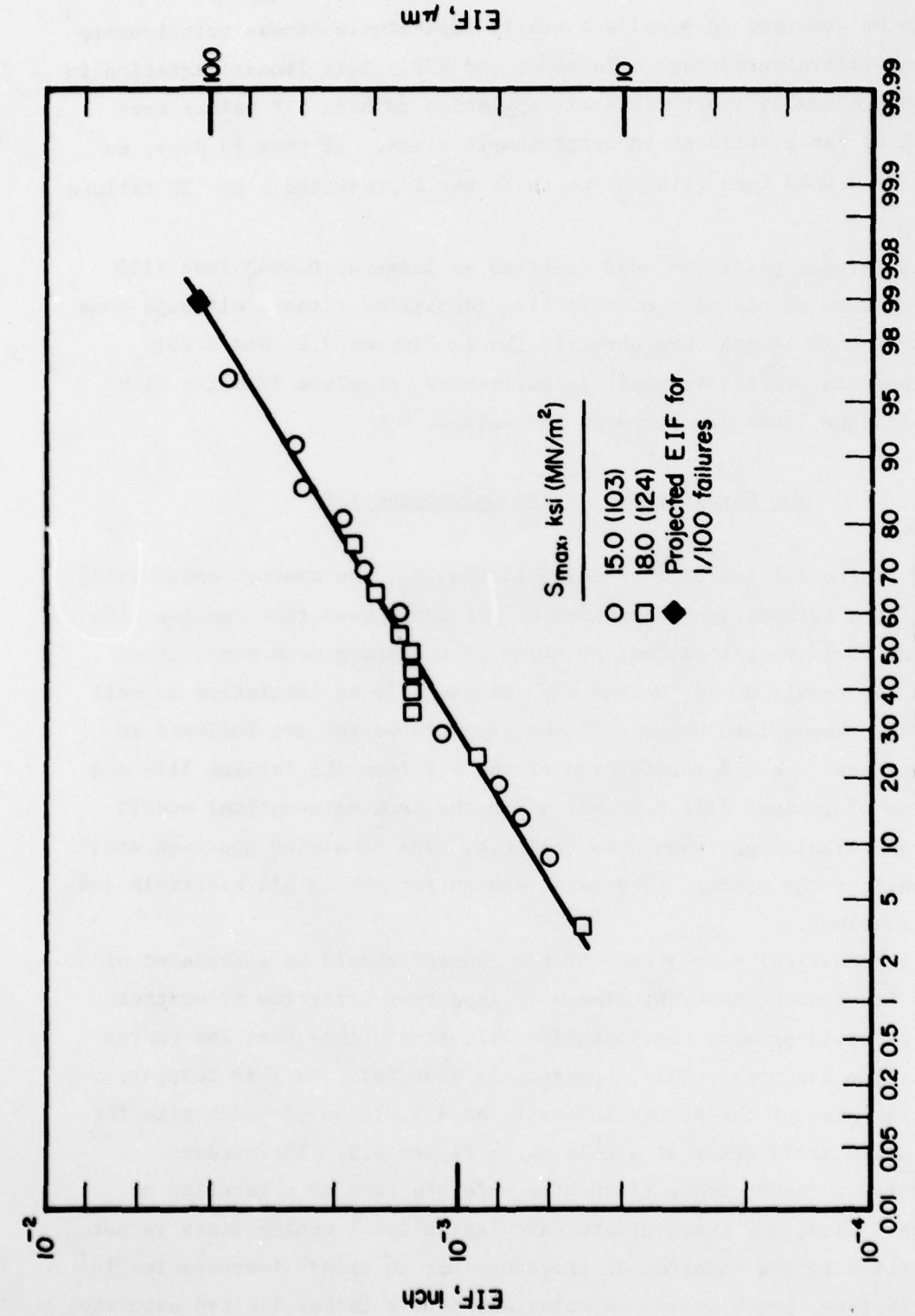

FIGURE 3.4. EQUIVALENT INITIAL FLAW CUMULATIVE PERCENTAGE

the data were generated at two different stress levels, the computed EIF values can be combined to provide a nearly logarithmic-linear relationship between cumulative percentage occurrence and EIF. This linear variation in EIF allows reasonable short-range extrapolation to high EIF values corresponding to early failures in large sample sizes. If this is done, an EIF of about 0.0043 inch (110 μm) is found for a projected 1 in 100 failure occurrence.

No individual particles were observed as large as 0.0043 inch (110 μm). There were no clusters of this size identified either, although some stringers of this length were observed (as in Figures 2.22 and 2.23). None of these intermetallic particle parameters correlate directly with observed fatigue lives and computed EIF values.

The Significance of the Calculated EIF

Even if the EIF has no real physical meaning, the concept could still be of use as a mathematical convenience. It would mean that fatigue life to fracture could be calculated, by means of a crack-growth computation only, and the result would include the fatigue life to initiation as well as the crack-propagation phase. If the same procedures are followed in both directions (i.e., determination of the EIF from the fatigue life and calculation of fatigue life from EIF using the same mathematical model) the fatigue calculations should be reliable. The remaining question would then be whether the concept is general enough for use in all materials and in all situations.

The mathematical convenience of the concept should be considered of secondary importance, however. The more important criterion is whether the concept would provide more accurate life predictions than the conventional fatigue analysis. This, however, is doubtful. In this respect, consider the plot of the stress intensity as a function of crack size for a center crack and a crack at a hole as in Figure 3.5. The stress intensity for a center crack rises at a moderate rate as a function of crack size. Thus, the crack-growth calculation for a center crack is not very sensitive to the integration procedure nor to slight inaccuracies in K. Nevertheless, crack growth calculations have a rather limited accuracy.

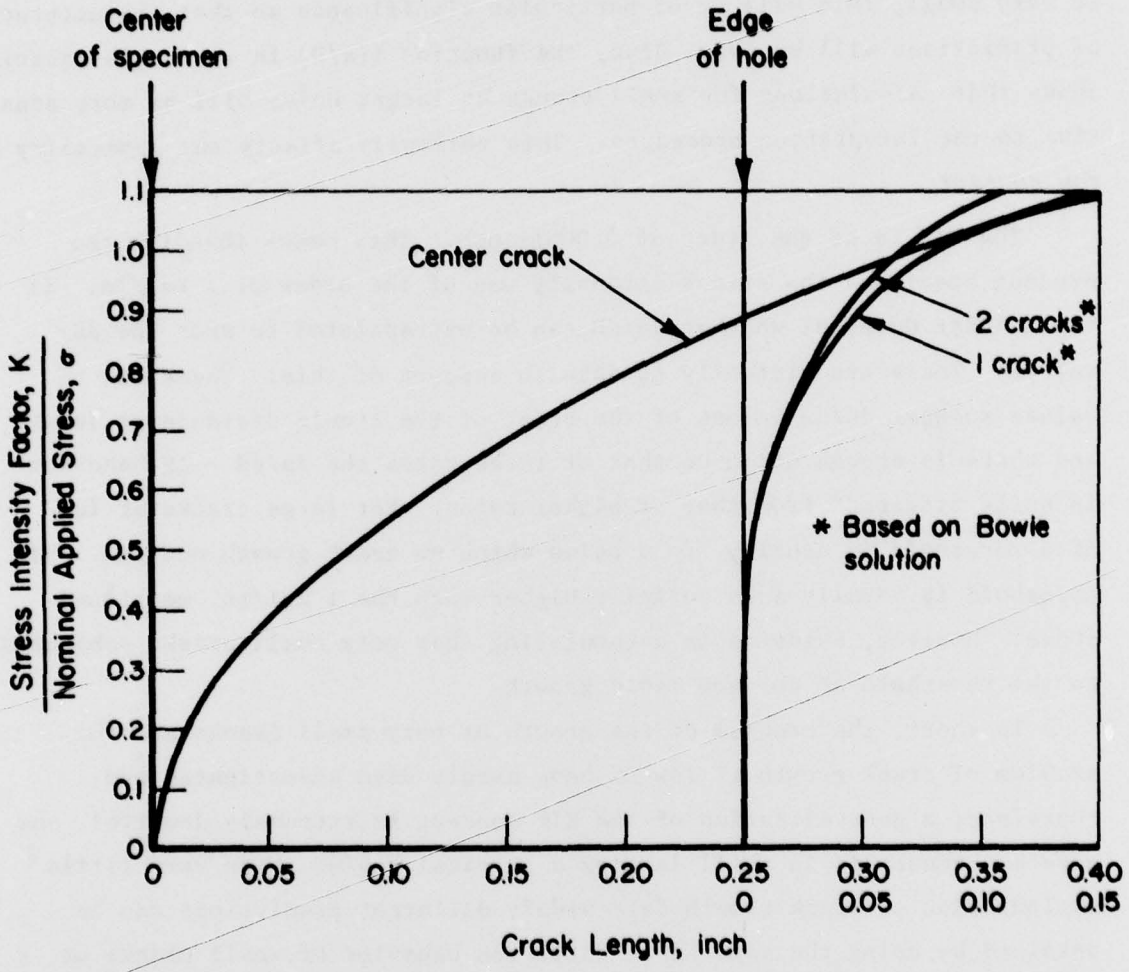

FIGURE 3.5. STRESS INTENSITY FOR A CRACK EMANATING FROM A 0.5-INCH DIAMETER HOLE

In comparison, the K-curve for a crack at a hole rises extremely sharply in the regime of small cracks. As a result, the calculation will be extremely sensitive to the integration procedure and to errors in K. Since the EIF is very small, this will be of particular significance so that the accuracy of predictions will be low. Also, the function f(a/D) in the Bowie equation shows that calculations for small cracks at larger holes will be more sensitive to the integration procedure. This seriously affects the generality of the concept.

The EIF is of the order of 0.0001-inch. This means that for the present specimens the stress intensity was of the order of 1 ksi$\sqrt{in}$. It is at least doubtful whether da/dN can be extrapolated to such low ΔK-values. There are virtually no data in support of this. These low ΔK values suggest da/dN values of the order of the atomic distance or less, and there is enough evidence that at these rates the da/dN - ΔK behavior is quite different from that at higher rates. For large cracks at low ΔK a threshold is usually found below which no crack growth occurs. This threshold is usually substantially higher than the 1 ksi$\sqrt{in}$. mentioned above. However, evidence is accumulating that very small cracks subjected to the threshold ΔK do show rapid growth.

In short, the problem of the growth of very small cracks and the problem of crack growth at low ΔK have hardly been investigated and, therefore, a generalization of the EIF concept is extremely doubtful, the more so because it is still lacking a physical basis. With very little manipulation of crack growth data widely different predictions can be obtained by using the same EIF. Until the behavior of small cracks at low ΔK has been studied more extensively, there is no acceptable rationale to treat the problem.

4. CONCLUSIONS

Based on the results of this research program, two major conclusions have been made as follows:

- There is not an apparent physical link between an EIF and intermetallic particle statistics.

- Definition of an empirical EIF is possible based upon a ranking of crack initiation data. Values around 0.004 to 0.005 inch (100 to 125 μm) appear to relate to a 99 percent survival level for the specimen tested. Computed EIF values for actual experimental results ranged from 0.0005 to 0.0036 inch (13 to 90 μm).

5. REFERENCES

1. Grosskreuts, G. C., and Shaw, G. C., Critical Mechanisms in the Development of Fatigue Cracks in 2024-T4 Aluminum Fracture, Chapman and Hall (1969) p 620.

2. Bowles, C. Q., and Schijve, J., "The Role of Inclusions in Fatigue Crack Initiation in an Aluminum Alloy", Int. J. Fract. Mech., 9, (171) (1972).

3. Broek, D., "Some Contributions of Electron Fractography to the Theory of Fracture", Int. Met. Reviews, 19, (135) (1974).

4. Broek, D., "A Study on Ductile Fracture", NLR Report No. TR-71021 (1971).

5. Peterson, R. E., Stress Concentration Design Factors, J. Wiley, New York, Chapman and Hall, London (1953).

6. Anon., "F/Rf-4 C/D Damage Tolerance and Life Assessment Study", McDonnell Report No. A2883 (1974).

7. Grandt, A. F., Jr., "A General Stress Intensity Factor Solution for Through-Cracked Fastener Holes", Submitted for publication in Int. J. of Fracture.

8. Noronhu, P. J., Fastener Hole Quality Industry Debriefing, Sept. 26, 1978.

DISTRIBUTION LIST

	No. of Copies
NAVAIRSYSCOM, AIR-50174 (2 for retention, 2 for AIR-530, 1 for AIR-530215, 1 for AIR-530221C, 2 for AIR-320B)	8
NAVAIRTESTCEN, Patuxent River, Maryland	1
NAVAVNSAFECEN, NAS, Norfolk, Virginia	1
CNAVANTRA, NAS, Corpus Christi, Texas	1
CNABATRA, NAS, Pensacola, Florida	1
CNARESTRA, NAS, Glenview, Illinois	1
CNATRA, NAS, Pensacola, Florida	1
NAVAIRSYSCOMREPLANT	1
NAVAIRSYSCOMREPCENT	1
NAVAIRSYSCOMREPAC	1
NAVAIREWORKFAC, NAS, Alameda, California	1
NAVAIREWORKFAC, NAS, Jacksonville, Florida	1
NAVAIREWORKFAC, NAS, Norfolk, Virginia	1
NAVAIREWORKFAC, NAS, Pensacola, Florida	1
NAVAIREWORKFAC, NAS, Quonset Point, Rhode Island	1
NAVAIREWORKFAC, NAS, San Diego, California	1
NAVAIREWORKFAC, NAS, Cherry Point, North Carolina	1
COMNAVAIRLANT	1
COMNAVAIRPAC	1
NWL, Dahlgren, Virginia (Attention Mr. Morton)	1
USAF Systems Command, WPAFB, Ohio 45433	
Attention FBR	1
Attention FB	1
Attention LLD	1
Attention SEFS	1
Attention FYA	1
Attention LAM	1
Attention FBA	1
Attention LPH	1
USA AMMRC, Watertown, Massachusetts	1
USA APG, Aberdeen, Maryland	1
USA AMRDL, Fort Eustis, Virginia (Attention Mr. Berrisford)	1
USA AVSCOM, St. Louis, Missouri (Attention AMSAV-GR)	1
Defense Research and Development Staff, British Embassy, Washington, D.C., via NAVAIR (AIR-5302)	1
Canadian Joint Staff, Navy Member, Washington, D.C., via NAVAIR (AIR-5302)	1
Technical Advisory, AF1AS-B, Directorate of Aerospace Safety, Norton AFB, California	1
DDC	12
NAVSEASYSCOM, Washington, D.C. 20362 (Attention Mr. C. Pohler, Code 035)	1
NAVSHIPRADCEN, Bethesda, Maryland 20034 (Attention Mr. A. B. Stavovy 730)	1
Bell Aerosystems Co., Buffalo, New York 14205	1
Bell Helicopter Co., Fort Worth, Texas 76101	1
Boeing Co., Airplane Div., Seattle, Washington 98124 (Attention Mr. T. Porter)	1

DISTRIBUTION LIST (continued)

	No. of Copies
Boeing Co., Airplane Div., Wichita, Kansas 67210	1
Boeing Co., Vertol Div., Philadelphia, Pennsylvania 19142	1
McDonnell Douglas Aircraft Corp., Aircraft Div., Long Beach, California 90801	1
General Dynamics/Convair, San Diego, California 92112	1
General Dynamics Corp., Fort Worth, Texas 76101	1
Goodyear Aerospace Corp., Akron, Ohio 44305	1
Grumman Aerospace Corp., Bethpage, Long Island, New York 11714	1
Aircraft-Missiles Div., Fairchild-Hiller Corp.,	1
Hagerstown, Maryland 21740	1
Kaman Aircraft Corp., Bloomfield, Connecticut 06002	1
Lockheed Aircraft Corp., Lockheed-California Co., Burbank, California 91503	1
Lockheed Aircraft Corp., Lockheed-Georgia Co., Marietta, Georgia 30061	1
LTV Aerospace Corp., Dallas, Texas 75222	1
Martin Co., Baltimore, Maryland 21203	1
McDonnell Douglas Aircraft Corp., St. Louis, Missouri 63166	1
Rockwell International, Columbus Aircraft Div., Columbus, Ohio 43216 (Attention Mr. O. Acker)	1
Rockwell International, Los Angeles, California 90053 (Attention Mr. G. Fitch)	1
Northrop Corp., Aircraft Div., Hawthorne, California 90250	1
Republic Aviation Div., Fairchild-Hiller Corp., Farmingdale, Long Island, New York 11735	1
Sikorsky Aircraft Co., Stratford, Connecticut 06497	1
Hdqtrs., R&T Div., AFSC, Bolling AFB, Washington, D.C. 22209	1
Office of Aerospace Research, Arlington, Virginia 22209	1
FAA (FS-120), Washington, D.C., 20553	1
Scientific and Technical Information Facility, College Park, Maryland 20740 (NASA Rep.)	2
Administrator, NASA, Washington, D.C. 20546	1
NASA-Langley Research Center, Materials Div., Hampton Virginia 23365 (Attention Mr. H. F. Hardrath)	1
National BuStds, Washington, D.C. 20234	1
Office of Naval Research, Washington, D.C. 20362 (Attention Dr. N. Perrone)	1
Director, Naval Research Lab, Washington, D.C. 20390	1
Midwest Research Institute, Kansas City, Missouri 64110	1
University of Illinois, Urbana, Illinois 61803 (Attention Prof. T. J. Dolan and Prof. J. Morrow)	1 each
University of Kansas, Lawrence, Kansas 66044	1
University of Michigan, Ann Arbor, Michigan 48105	1
University of Minnesota, Minneapolis, Minnesota 55455	1
Alcoa, Alcoa Labs, Alcoa Center, Pennsylvania 15069 (Attention Mr. J. G. Kaufman)	1
Lehigh University, Bethlehem, Pennsylvania 18015 (Attention Prof. G. C. Sih)	1
Belfour-Stulen, Inc., Traverse City, Michigan 49684	1
Cornell Aero. Lab, Buffalo, New York 14221	1

DISTRIBUTION LIST (continued)

	No. of Copies
Metals & Ceramics Information Center, Battelle, Columbus Laboratories Columbus, Ohio 43201	1
NASA, Lewis Research Center, Cleveland, Ohio 44153 (Attention Technical Library)	1
Naval Postgraduate School, Monterey, California 93940 (Attention Prof. Lindsey)	1
Battelle, Pacific Northwest Laboratories, P. O. Box 999, Richland, Washington 99352 (Attention Mr. W. E. Anderson)	1
School of Engineering, George Washington University, Washington, D.C. 20006 (Attention Prof. H. Liebowitz)	1
Dept. of Metallurgy, University of Connecticut, Storrs, Connecticut 06268 (Attention Prof. A. J. McEvily)	1
Dept. of Mech. Eng., Washington University, St. Louis, Missouri (Attention Prof. P. C. Paris)	1
Materials Dept., 6531 Boelter Hall, University of California at Los Angeles, Los Angeles, California 90024 (Attention Prof. A. S. Tetelman)	1
National Transportation Safety Board, 800 Independence, Washington, D.C. 20594 (Attention Mr. W. D. Cowan)	1
Federal Aircraft Establishment, Emmen, Switzerland (Attention Mr. J. Branger)	1
Civil Aviation Authority, Structures Section, Brabaron House, Redhill, Surrey RH11SQ, England (Attention Mr. M. B. Benoy)	1
Royal Aircraft Establishment, Structures Dept., Farnborough, Hants GU146TD, England (Attention Mr. W. T. Kirkby)	1
Aeronautical Research Labs, Melbourne, Australia (Attention Mr. J. Y. Mann)	1
DFVLR, 505 Pors Wahn, West Germany (Attention Dr. H. Nowack)	1
Pratt and Whitney Aircraft, P. O. Box 611, Middletown, Connecticut (Attention Mr. C. A. Rau)	1
IABG, 8012 Ottobrunn by Munich, West Germany (Attention Dr. W. Schutz)	1
Aeronautics Dept., Delft University, Delft, Holland (Attention Prof. J. Schijve)	1
National Aerospace Inst., NLR, Emmeloord, Holland (Attention Mr. J. B. deJonge)	1
Federal Aviation Administration, RLD, Schiphol, Holland (Attention Mr. H. N. Wolleswinkel)	1
Royal Aeronautical Society, 4 Hamilton Place, London, England (Attention Mr. E. R. Welbourne)	1
Service Technique Aeronautique, 4 Ave de la Porte d'Issy, Paris 15, France (Attention Mr. G. Bessonat)	1
British Aircraft Corporation, Commercial AC Div., Filton House, Bristol BS99 7AR, England (Attention Mr. N. F. Harpur)	1
Fokker-VFW Aircraft Co., Schiphol, Netherlands (Attention Mr. G. Fonk)	
FAA, 800 Independence, Washington, D. C. 20594 (Attention Mr. D. Kemp)	1
University of Tennessee Space Inst., Tullahoma, Tennessee 37388 (Attention Prof. M. A. Wright)	1
Shell Oil Company, Civil Engineering Office, P. O. Box 2099, Houston, Texas 77001 (Attention Mr. P. W. Marshall)	1
David Taylor Naval Ship Research and Development Center, Bethesda, Maryland 20084 (Attention Mr. J. Corado)	1

DISTRIBUTION LIST (continued)

	No. of Copies
Air Force Flight Dynamics Lab, WPAFB, Ohio 45433 (Attention Mr. R. M. Engle)	1
Vanderbilt University, P. O. Box 3245 Station B, Nashville, Tennessee 37235 (Attention Prof. P. Packman)	1
Dept. of Civil Aviation, P. O. Box 1733 P, Melbourne 3001, Australia (Attention Mr. M. R. Rice)	1
University of Dayton Research Institute, 300 College Park, Dayton, Ohio 45469 (Attention Dr. Joseph Gallagher, Group Leader Service Life Management).	1